

TOP PHYSICS*

ELIZABETH H. SIMMONS

Department of Physics, Boston University
590 Commonwealth Avenue, Boston, MA 02215, USA
and
Radcliffe Institute for Advanced Study, Harvard University
34 Concord Avenue, Cambridge, MA 02138
e-mail: simmons@bu.edu

The Run I experiments at the Fermilab Tevatron Collider discovered the top quark and provided first measurements of many of its properties. Run II (and eventually the LHC and NLC experiments) promise to extend our knowledge of the top quark significantly. Understanding the top quark's large mass, and indeed the origin of all mass, appears to require physics beyond the Standard Model. Thus, the top quark may have unusual properties accessible to upcoming experiments.

1 Within the Standard Model

The three-generation Standard Model (SM) of particle physics came into existence with the discoveries of the tau lepton¹ and b quark.² Completing the model required a weak partner for b. Several important properties of this hypothetical "top" quark could be deduced from measurements of bottom quark characteristics. The electric charge of the b quark was related to the ratio

$$R = \frac{\sigma(e^+e^- \rightarrow \text{hadrons})}{\sigma(e^+e^- \rightarrow \mu^+\mu^-)} = \Sigma_q (3Q_q^2). \quad (1)$$

The increment in the measured³ value $\delta R^{expt} = 0.36 \pm 0.09 \pm 0.03$ at the b threshold agreed with the predicted $\delta R^{SM} = \frac{1}{3}$, confirming $Q^b = -\frac{1}{3}$. Likewise, data⁴ on the front-back asymmetry for electroweak b-quark production

$$A_{FB} = \frac{\sigma(b, \theta > 90^\circ) - \sigma(b, \theta < 90^\circ)}{\sigma(b, \theta > 90^\circ) + \sigma(b, \theta < 90^\circ)} \quad (2)$$

where θ is the angle between the incoming electron and outgoing b quark, showed $A_{FB}^{expt} = -(22.8 \pm 6.0 \pm 2.5)\%$ while $A_{FB}^{SM} = -.25$ was predicted. Since the $Zb\bar{b}$ coupling depends on the weak isospin of the b quark, the measurement confirmed that $T_3^b = -\frac{1}{2}$. Therefore, the b quark's weak partner in the SM was required to be a color-triplet, spin- $\frac{1}{2}$ fermion with electric charge $Q = \frac{2}{3}$ and weak charge $T_3 = \frac{1}{2}$.

*Lectures presented at TASI 2000, *Flavor Physics for the Millennium*, June 4-30, 2000, University of Colorado, Boulder, CO. Preprint number BUHEP-00-23.

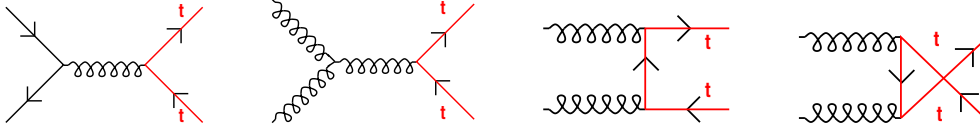


Figure 1. Feynman diagrams for QCD pair-production of top quarks.

Such a particle is readily pair-produced by QCD processes involving quark/anti-quark annihilation or gluon fusion, as illustrated in Figure 1. At the Tevatron’s collision energy $\sqrt{s} = 1.8$ TeV, a 175 GeV top quark is produced 90% through $q\bar{q} \rightarrow t\bar{t}$ and 10% through $gg \rightarrow t\bar{t}$; at the LHC with $\sqrt{s} = 14$ TeV, the opposite will be true. This is because the incoming partons must carry a momentum fraction of order m_t/E_{beam} , a large fraction at the Tevatron and a small one at LHC, and because the parton distribution function of gluons is softer than that of valence quarks. Note that had the size of m_t been different, weak (single top) production would have rivaled QCD (pair) production: for $m_t \sim 60$ GeV, the process $q\bar{q} \rightarrow W \rightarrow t\bar{b}$ is competitive while for $m_t \sim 200$ GeV, $Wg \rightarrow t\bar{b}$ dominates.⁵

In the three-generation SM, the top quark decays primarily to $W + b$ because $|V_{tb}| \approx 1$. As the W can decay into leptons or hadrons, there are three main classes of final states from top pair production. In the “dilepton” events (5% of all $t\bar{t}$ events), both W ’s decay to $\ell\nu_\ell$ (where $\ell \equiv e, \mu$) and the event includes two b-jets, two leptons and missing energy from two neutrinos. In the “lepton+jets” events (30%), there are two b-jets, two other jets from W decay, one energetic lepton, and missing energy. The “all jets” events (44%) have multiple jets (including 2 b-jets) and no hard leptons. The remaining 21% of events would include tau leptons which are harder to identify in high-energy hadron collider experiments.

In 1995, the CDF⁶ and DØ⁷ experiments at Fermilab discovered a new particle answering the above description and having a pair-production cross-section consistent with that predicted for a SM top quark with $m_t = 175$ GeV. During Tevatron Run I, each experiment gathered $\approx 125 \text{ pb}^{-1}$ of integrated luminosity, measured some top quark properties in detail and took a first look at others. In this section of the talk, we will review the measured characteristics of the top quark, considered primarily as a Standard Model particle^a. We will discuss the Run I results on the top quark mass, width, pair and single production cross-sections, spin correlations, and decays. We

^aAnother useful reference on this topic is ref.⁸

Table 1. Measured¹¹ m_t and σ_{tt} from CDF and DØ.

experiment	channel	m_t (GeV)	σ_{tt} (pb)
CDF	dilepton	167.4 ± 11.4	$8.4^{+4.5}_{-3.5}$
	lepton + jets	175.9 ± 7.1	5.1 ± 1.5 9.2 ± 4.3 (SVX b-tag) (soft lepton tag)
	all jets	186.0 ± 11.5	$7.6^{+3.5}_{-2.7}$
	combined	176.0 ± 6.5	$6.5^{+1.7}_{-1.4}$ ($m_t = 175$)
DØ	dilepton	168.4 ± 12.8	
	lepton + jets	173.3 ± 7.8	4.1 ± 2.1 8.3 ± 3.6 (topological) (soft lepton tag)
	all jets		7.1 ± 3.2
	combined	172.1 ± 7.1	5.9 ± 1.7 ($m_t = 172$)
Tevatron	combined	174.3 ± 5.1	

will also describe the increases in measurement precision anticipated at Run II and future accelerators and discuss what we hope to learn.

1.1 Mass

The top quark mass has been measured^{9,10} by reconstructing the decay products of top pairs produced at the Tevatron. The most precise measurements use lepton+jets decay channel which affords both a large top branching fraction and full event reconstruction. The combined measurement from CDF and DØ is $m_t = 174.3 \pm 5.1$ GeV, as shown in Table 1. This implies that the top Yukawa coupling $\lambda_t = 2^{3/4} G_F^{1/2} m_t$ is approximately 1, so that the top is the only quark to have a Yukawa coupling of “natural” size.

The top quark’s mass is already known to $\pm 3\%$, comparable to the precision with which m_b is measured and better than that for the light quarks.¹²



Figure 2. Examples of SM radiative corrections sensitive to m_t : (left) $\Delta\rho$ (right) $Zb\bar{b}$.

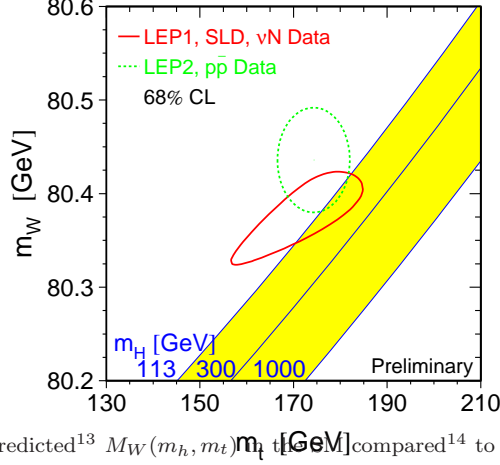


Figure 3. Predicted¹³ $M_W(m_h, m_t)$ compared¹⁴ to data on M_W, m_t .

This is quite impressive given that the top quark was discovered nearly 20 years after the bottom! This precision is also quite useful in interpreting other measurements because many electroweak observables are subject to radiative corrections sensitive to m_t . As illustrated in Figure 2, for example, the W mass (which enters $\Delta\rho$) and the $Zb\bar{b}$ coupling (which enters R_b) are affected by virtual top quarks. Comparing the experimental constraints on M_W and m_t with the SM prediction¹³ for $M_W(m_t, m_{Higgs})$ provides an opportunity to test the consistency of the SM and to constrain m_{Higgs} . As Figure 3 shows, the current data are suggestive, but not precise enough to provide a tightly-bounded value for m_{Higgs} . Run II measurements of the W and top masses are expected¹¹ to yield $\delta M_W \approx 40$ MeV (per experiment) and $\delta m_t \approx 3$ GeV (1 GeV in Run IIb or LHC). With this precision, it should be possible to obtain a much tighter bound¹¹ on the SM Higgs mass: $\delta M_H/M_H \leq 40\%$.

A far more precise measurement, with $\delta m_t \approx 150$ MeV, could in principle be extracted from near-threshold NLC¹⁵ data on $\sigma(e^+e^- \rightarrow t\bar{t})$. The calculated line shape shows a distinct rise at the remnant of what would have been the toponium 1S resonance if the top did not decay so quickly. The location of the rise depends on m_t ; the shape and size, on the decay width Γ_t . This measurement has the potential for good precision because it is based on counting color-singlet $t\bar{t}$ events, making it relatively insensitive to QCD uncertainties.

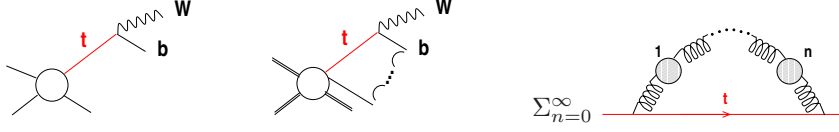


Figure 4. (left) Top production and decay. (center) Same, with b-quark hadronization indicated. (right) Soft gluon resummation in the top propagator. After ref. ¹⁶.

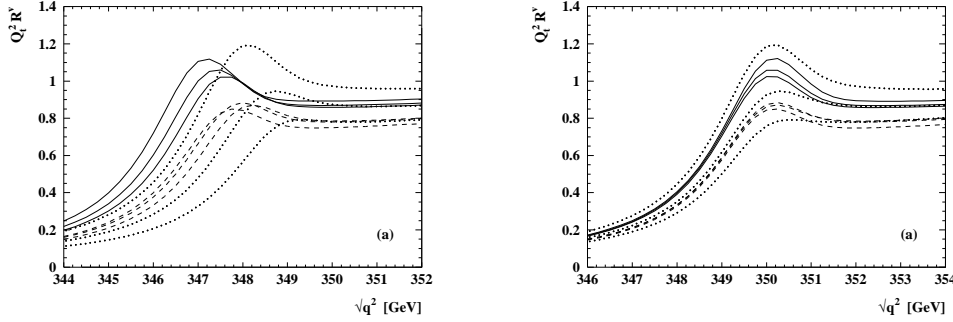


Figure 5. Near-threshold cross-section for photon-induced top production at an NLC²² calculated (left) in the pole mass scheme and (right) in the 1S mass scheme. Leading-order (dotted), NLO (dashed) and NNLO (solid) curves are shown with renormalization scales $\mu = 15$ (topmost), 30, and 60 GeV

Taking advantage of this requires a careful choice of the definition of m_t used to extract information from the data. Consider, for example, the mass appearing in the propagator $D(p) = i/(\not{p} - m_R - \Sigma(p))$. In principle, one can reconstruct this mass from the four-vectors of the top decay products, as is done in the current Tevatron measurements. But this pole mass is inherently uncertain to $\mathcal{O}(\Lambda_{QCD})$. For example, the clean top production and decay process sketched in Figure 4(left) is, in reality, complicated by QCD hadronization effects which connect the b-quark from top decay to other quarks involved in the original scattering,¹⁶ as in Figure 4(center). Attempting to sum the soft-gluon contributions to the top propagator sketched in Figure 4 (right) yields the same conclusion. Taking the Borel transform of the self-energy allows one to effect the summation,¹⁷ but real-axis singularities (infrared renormalons) in the Borel-transformed self-energy impede efforts to invert the transform.¹⁶ The ambiguity introduced in distorting the integration contour of the inverse Borel transform around the singularities is of order¹⁸ Λ_{QCD} .

Using a short-distance mass definition avoids these difficulties.¹⁹ For ex-

ample, one could adopt the \overline{MS} mass definition

$$\bar{m}(\bar{m}) = m_{pole} \left(1 + \frac{4\bar{\alpha}_s}{3\pi} + 8.3 \left(\frac{\bar{\alpha}_s}{\pi} \right)^2 + \dots \right)^{-1} \quad (3)$$

although the numerical value lies about 10 GeV below m_{pole} , which is inconvenient for data analysis. Another is the 1S mass²²

$$m_{1S} = m_{pole} - \frac{2}{9} \alpha_s^2 m_{pole} + \dots \quad (4)$$

where $2m_{1S}$ is naturally near the peak of $\sigma(e^+e^- \rightarrow t\bar{t})$. Others include the potential-subtracted²⁰ or kinetic²¹ masses. Figure 5 compares the photon-induced $t\bar{t}$ cross-section near threshold as calculated in the pole mass and 1S mass schemes (for $m_t = 175$ GeV and $\Gamma_t = 1.43$ GeV). In the pole mass scheme, the location and height of the peak vary with renormalization scale and order in perturbation theory; this choice introduces QCD uncertainties into what should be a color-singlet process. Using the short-distance mass renders the peak location stable and large higher-order corrections are avoided.

1.2 Top Decay Width

In the 3-generation SM, data on the lighter quarks combined with CKM matrix unitarity implies¹² $0.9991 < |V_{tb}| < 0.9994$. Thus the top decays almost exclusively through $t \rightarrow Wb$. At tree level, in the approximation where $M_W = m_b = 0$ and setting $|V_{tb}| = 1$, the decay width is

$$\Gamma_o(t \rightarrow Wb) \equiv \frac{G_F m_t^3}{8\pi\sqrt{2}} = 1.76 \text{ GeV} . \quad (5)$$

More precise calculations yield similar results. Including $M_W \neq 0$ gives

$$\Gamma_t/|V_{tb}|^2 = \Gamma_o \left(1 - 3 \frac{M_W^4}{m_t^4} + 2 \frac{M_W^6}{m_t^6} \right) = 1.56 \text{ GeV} . \quad (6)$$

while including the b-quark mass and radiative corrections refines this to²³ $\Gamma_t/|V_{tb}|^2 = 1.42 \text{ GeV}$.

As a result, the top decays in $\tau_t \approx 0.4 \times 10^{-24}$ s. Since this is appreciably shorter than the characteristic QCD time scale $\tau_{QCD} \approx 3 \times 10^{-24}$ s, the top quark decays before it can hadronize. Therefore, unlike the b and c quarks which offer rich spectra of bound states for experimental study, the top quark is not expected to provide any interesting spectroscopy.

A precise measurement of the top quark width could, in principle, be made at an NLC running at $\sqrt{s} \sim 350$ GeV by exploiting the fact that Γ_t controls the threshold peak height in $\sigma(e^+e^- \rightarrow t\bar{t})$. Until recently, the NNLO

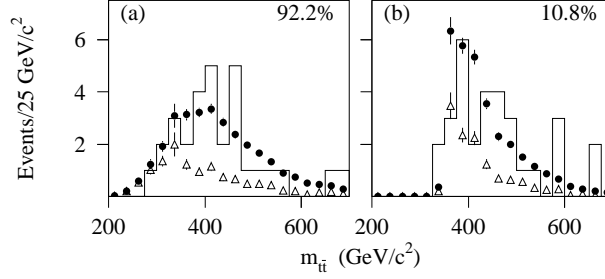


Figure 6. Invariant mass distribution¹⁰ for top pairs: DØ data (histogram), simulated background (triangles), simulated S+B (dots). In (a) m_t unconstrained; in (b) $m_t = 173$ GeV.

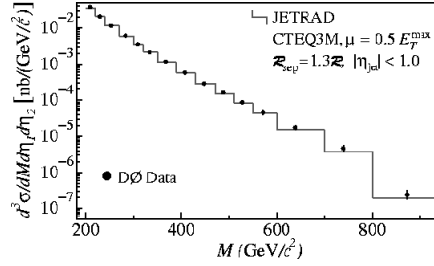


Figure 7. Light dijet invariant mass distribution²⁸: prediction (solid) and DØ data (dots).

calculations were plagued by a 20% normalization ambiguity which made the realization of this aim uncertain;¹⁹ preliminary new results²⁴ suggest the issue has been favorably resolved.

1.3 Pair Production

The top pair production cross-section has been measured in all available channels by CDF²⁵ and DØ.²⁶ As with m_t , the lepton+jets channel, with its combination of statistics and full reconstruction, gives the single most precise measurement (see Table 1). The combined average of $\sigma_{tt}(m_t = 172 \text{ GeV}) = 5.9 \pm 1.7 \text{ pb}$ is consistent with SM predictions including radiative corrections.²⁷

Initial measurements of the invariant mass (M_{tt}) and transverse momentum (p_T) distributions of the produced top quarks have been made, as shown in Figure 6. While a comparison with the measured M_{jj} distribution for

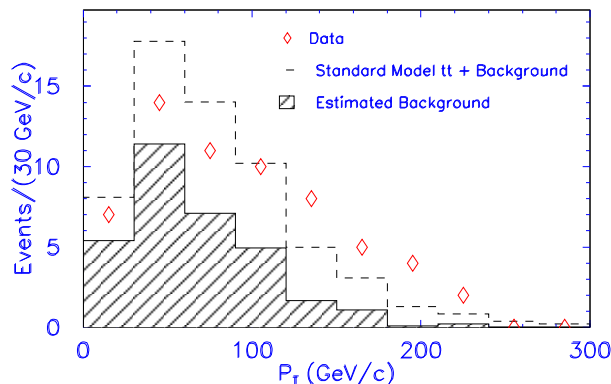


Figure 8. p_T distribution for hadronically-decaying tops in lepton+jets events from CDF.³⁰

QCD dijets (Figure 7) illustrates how statistics-limited the Run I top sample is, some preliminary limits on new physics are being extracted. It has been noted, e.g. that a narrow 500 GeV Z' boson is inconsistent with the observed shape of the high-mass end of CDF's $M_{t\bar{t}}$ distribution.²⁹ The p_T distribution for the hadronically-decaying top in fully-reconstructed lepton + jets events (Figure 8) constrains non-SM physics which increases the number of high- p_T events. The fraction $R_4 = 0.000^{+0.031}_{-0.000}(stat)^{+0.024}_{-0.000}(sys)$ of events in the highest p_T bin ($225 \leq p_T \leq 300$ GeV) implies³⁰ a 95% c.l. upper bound $R_4 \leq 0.16$ as compared with the SM prediction $R_4 = 0.025$.

In Run II, the $\sigma_{t\bar{t}}$ measurement will be dominated by systematic uncertainties; the collaborations will use the large data sample to reduce reliance on simulations.³¹ Acceptance issues such as initial state radiation, the jet energy scale, and the b-tagging efficiency will be studied directly in the data. The background uncertainty for the lepton+jets mode will be addressed by measuring the heavy-flavor content of W+jets events. It is anticipated³¹ that an integrated luminosity of 1 (10, 100) fb^{-1} will enable $\sigma_{t\bar{t}}$ to be measured to ± 11 (6, 5) %. The $M_{t\bar{t}}$ distribution will then constrain $\sigma \cdot B$ for new resonances decaying to $t\bar{t}$ as illustrated in Figure 9.

1.4 Spin Correlations

When a $t\bar{t}$ pair is produced, the spins of the two fermions are correlated.³² This can be measured at lepton or hadron colliders, and provides another means of testing the predictions of the SM or looking for new physics.

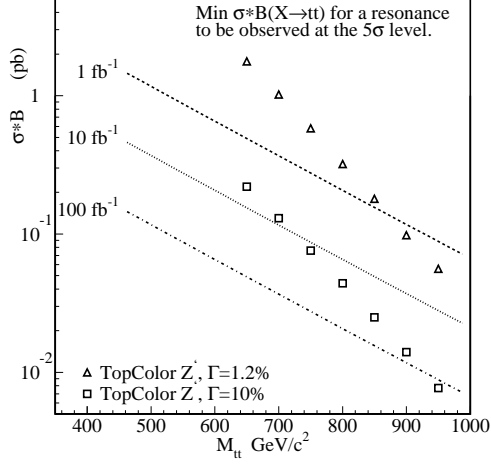


Figure 9. Anticipated³¹ Run II limits on $\sigma \cdot B(X \rightarrow t\bar{t})$.

One starts from the fact that the top quark decays before its spin can flip.³³ The spin correlations between t and \bar{t} therefore yield angular correlations among their decay products. If χ is angle between the top spin and the momentum of a given decay product, the differential top decay rate (in the top rest frame) is

$$\frac{1}{\Gamma} \frac{d\Gamma}{d \cos \chi} = \frac{1}{2} (1 + \alpha \cos \chi) \quad (7)$$

The factor α is computed³⁴ to be 1.0 (0.41, -0.31, -0.41) if the decay product is ℓ or d (W , ν or u , b). A final-state lepton is readily identifiable and has largest value of α ; thus, dilepton events are best for studying $t\bar{t}$ spin correlations.

Choosing a good basis along which to project the spin variables is key to extracting information from the data. For example, consider $e^+e^- \rightarrow t\bar{t}$ at the NLC. If the beams are polarized, using a helicity basis seems logical, but near the $t\bar{t}$ threshold helicity is not very useful. Fortunately, there is an optimal “off-diagonal” basis³⁵ which gives a clean prediction for spin correlations: in leading order the spins are purely anti-correlated ($t_{\uparrow}\bar{t}_{\downarrow} + t_{\downarrow}\bar{t}_{\uparrow}$). One projects the top spin along an axis identified by angle ψ

$$\tan \psi = \frac{\beta^2 \sin \theta^* \cos \theta^*}{1 - \beta^2 \sin^2 \theta^*} \quad (8)$$

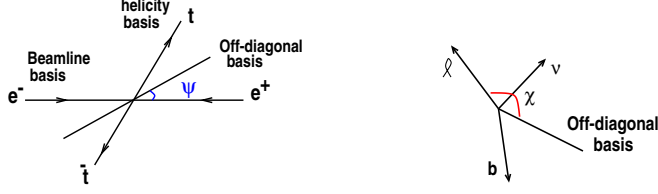


Figure 10. Definitions of the off-diagonal basis and decay lepton angles for studying top spin correlations.

where β is the top quark's speed in the center-of-momentum scattering frame and θ^* is the top scattering angle in that frame. The basis angle ψ and decay lepton angle χ are illustrated in Figure 10.

The advantages of an appropriate basis are clear from Figure 11: for a given data sample, discerning the clean predication of the off-diagonal basis should be far easier than untangling the several possible spin configurations in the helicity basis. Moreover, while the fraction of top quarks in the dominant spin configuration in $e_L^- e_R^+ \rightarrow t\bar{t}$ approaches unity in the helicity basis at large β , it is always nearly one in the off-diagonal basis (Figure 12).

This idea carries over to the Tevatron. In the helicity basis, 70% of $t\bar{t}$ pairs have opposite helicities³⁶: threshold production via $q\bar{q}$ annihilation puts the tops in a 3S_1 state³⁷ where their spins tend to be aligned. But the off-diagonal basis still does better³⁸: 92% of the top pairs have anti-aligned spins. The larger spin correlation translates into larger and more measurable correlations among the decay leptons. Writing the differential cross-section in terms of the angular positions χ^\pm of the decay leptons ℓ^\pm

$$\frac{1}{\sigma} \frac{d^2\sigma}{d(\cos\chi_+)d(\cos\chi_-)} = \frac{1}{4}(1 + \kappa \cos\chi_+ \cos\chi_-) \quad (9)$$

one finds $\kappa \approx 0.9$ in the SM for $\sqrt{s} = 1.8$ TeV. As DØ recorded only six dilepton events in Run I, they set³⁹ merely the 68% c.l. limit $\kappa \geq -0.25$. Nonetheless, the possibility of making a top spin correlation measurement in a hadronic environment has been established and Run IIa promises ~ 150 dilepton events.³¹

At the LHC, the top dilepton sample will be of order 4×10^5 events per year²³ – but no spin basis with nearly 100% correlation at all β has been identified. Pair production proceeds mainly through $gg \rightarrow t\bar{t}$, putting the tops in a 1S_0 state³⁷ at threshold. Near threshold, angular momentum conservation favors like helicities; far above threshold, helicity conservation favors opposite

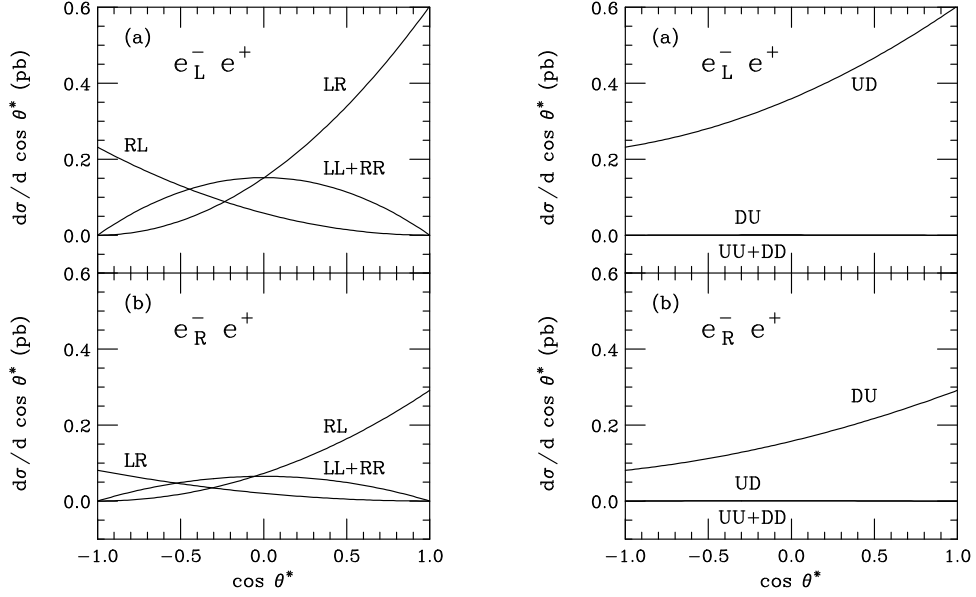


Figure 11. Differential cross-section for top production at 400 GeV NLC with³⁵ (a) LH and (b) RH electron beams. At left spins are projected onto the helicity basis; at right, onto the off-diagonal basis.

helicities.²³ In the helicity basis, one conventionally studies a differential cross-section of the same form as Eq. (9), in which the coefficient κ is renamed $-C$ and the angle χ_{\pm} refers to the angle between the t (\bar{t}) momentum in the center-of-momentum frame and the ℓ^{\pm} direction in the t (\bar{t}) rest frame. The SM predicts $C \approx 0.33$ in leading order at the LHC. Physically, C corresponds^b to the ratio³⁶

$$C = \frac{N(t_L \bar{t}_L + t_R \bar{t}_R) - N(t_L \bar{t}_R + t_R \bar{t}_L)}{N(t_L \bar{t}_L + t_R \bar{t}_R) + N(t_L \bar{t}_R + t_R \bar{t}_L)}. \quad (10)$$

The effects of radiative corrections and the likely measurement precision achievable remain to be evaluated.²³

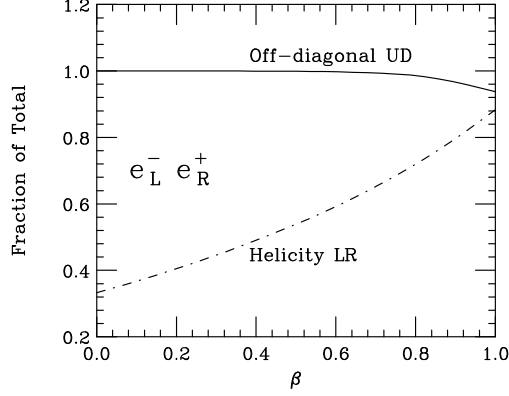


Figure 12. Fraction of top quarks in the dominant spin configuration³⁵ for $e_L^- e_R^+ \rightarrow t\bar{t}$.

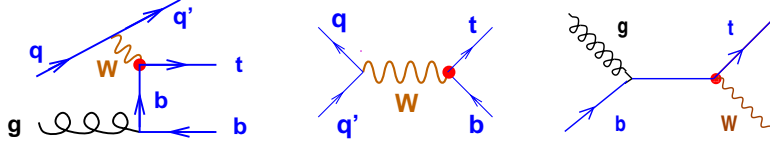


Figure 13. Feynman diagrams for single top quark production.

1.5 Single Production

The three SM channels for single top production are Wg fusion, $q\bar{q}$ annihilation through an off-shell W , and $gb \rightarrow tW$; the Feynman diagrams are shown in Figure 13. The Wg fusion events are characterized by one hard and one soft b -jet, an additional jet and a W ; the SM Run I cross-section is calculated⁴⁰ to be 1.70 ± 0.9 pb. The W^* events, in contrast, include two hard b quarks and a W from top decay; the calculated⁴⁰ SM Run I cross-section is $\sigma = 0.73 \pm 0.04$ pb. The $gb \rightarrow tW$ process is highly suppressed at the Tevatron.

Searches for single top production generally focus on leptonically-decaying W bosons. The principle backgrounds come from top pair production, W +jets events, QCD multijet events in which a jet fakes an electron, and WW events.

^bThis expression also holds for $-\kappa$ at the Tevatron if L and R are taken to refer to the off-diagonal rather than the helicity basis.

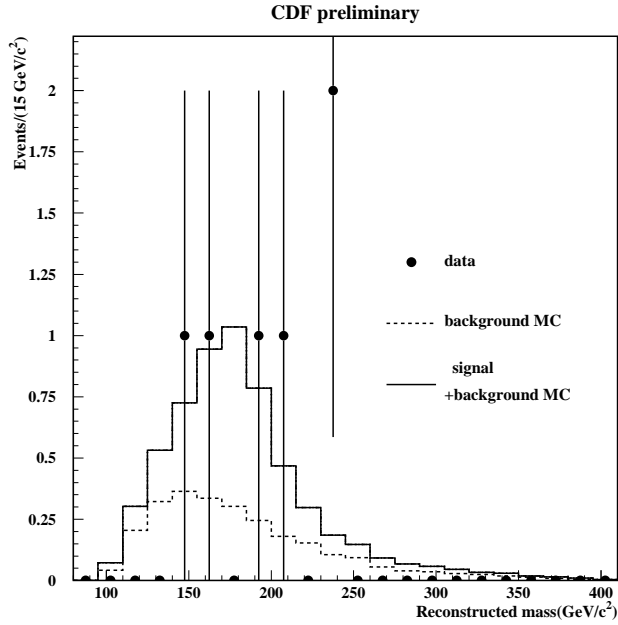


Figure 14. Reconstructed m_t for the CDF⁴² Wbb sample. “Signal” is single top production.

While the $D\bar{O}$ analysis of single top production is still in progress^c, CDF has set two limits.⁴² The first is based on reconstructing a top quark mass for the six events with Wbb identified in the final state, as illustrated in Figure 14. Using Run I data, CDF finds $\sigma_{tb} < 18.6$ pb (the SM prediction is 2.43 pb). The higher luminosity in Run II should provide $S/\sqrt{B} \geq 4$ in this channel. The second limit exploits the differences among the H_T distributions in signal and background W +jet events; H_T is the scalar sum of the jet, lepton, and missing transverse-energies. Each event is required to include 1-3 jets (one of which is b-tagged), a lepton from W decay, and a reconstructed top mass in the range 140 - 210 GeV. The cross-section limit set with Run I data shown in Figure 15 is $\sigma_{tb} < 13.5$ pb.

^cThe $D\bar{O}$ limit⁴¹ became available after these lectures were given. It is not stronger than the CDF limits.

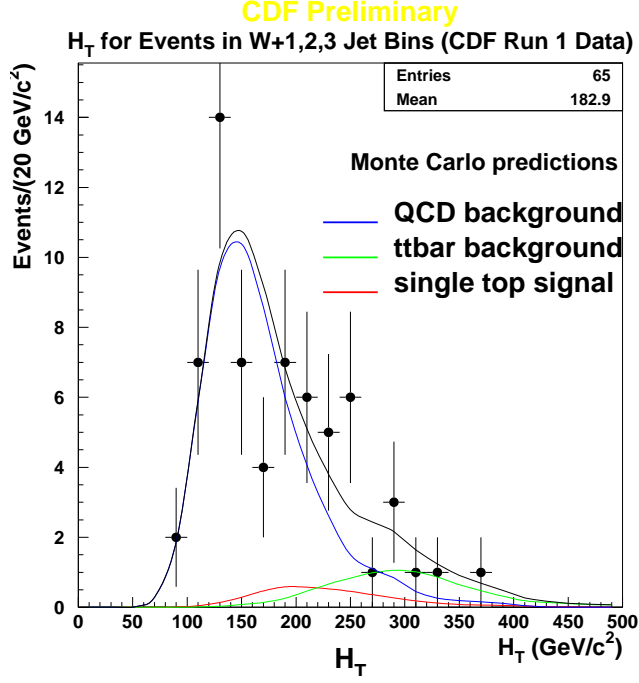


Figure 15. H_T distribution in single top production⁴²: CDF data and simulated backgrounds.

1.6 Decays

W helicity in top decay

The SM predicts the fraction (\mathcal{F}_0) of top quark decays to longitudinal (zero-helicity) W bosons will be quite large, due to the top quark's big Yukawa coupling:

$$\mathcal{F}_0 = \frac{m_t^2/2M_W^2}{1 + m_t^2/2M_W^2} = (70.1 \pm 1.6)\% . \quad (11)$$

One can measure \mathcal{F}_0 in dilepton or lepton+jet events by exploiting the correlation of the W helicity with the momentum of the decay leptons. For $W^+ \rightarrow \ell^+ \nu$, the spins of the decay leptons align with that of the W ; for massless leptons, the ℓ^+ (ν) momentum points along (opposite) its spin. Then a positive-helicity W (boosted along its spin) yields harder charged leptons than a negative-helicity W . The longitudinal W gives intermediate results.

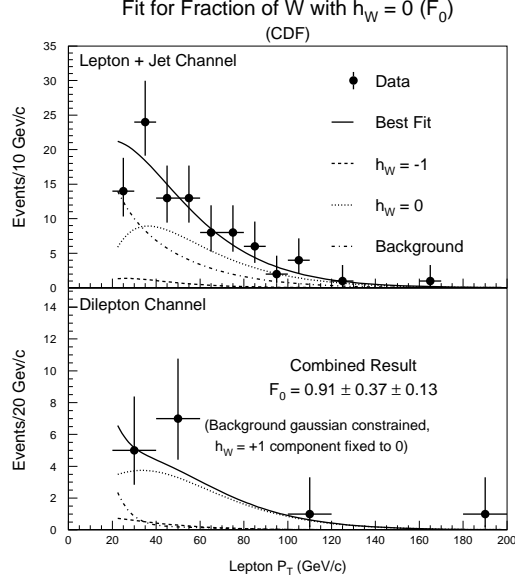


Figure 16. Measured lepton p_T spectra and fits to W helicity by CDF.⁴³

CDF has measured⁴³ the lepton p_T spectra for dilepton and lepton + jet events and performed fits as shown in Figure 16. There is insufficient data to permit forming conclusions about all three helicity states simultaneously. By assuming no positive-helicity W 's are present, CDF obtains the limit $\mathcal{F}_0 = 0.91 \pm 0.37 \pm 0.13$. By setting \mathcal{F}_0 to its SM value of 0.70, they obtain the 95% c.l. upper limit $\mathcal{F}_+ < 0.28$. Note, however, that the first limit essentially states only that no more than 100% of the decay W 's are longitudinal and the second, that no more than $1 - \mathcal{F}_0$ have positive helicity. More informative constraints are expected from Run II (see Table 2).

b quark decay fraction

Table 2. Predicted³¹ precision of Run II W helicity measurement for several $\int \mathcal{L} dt$.

	1 fb ⁻¹	10 fb ⁻¹	100 fb ⁻¹
$\delta\mathcal{F}_0$	6.5%	2.1%	0.7%
$\delta\mathcal{F}_+$	2.6%	0.8%	0.3%

The top quark's decay fraction to b quarks is measured by CDF⁴⁴ to be $B_b \equiv \Gamma(t \rightarrow bW)/\Gamma(t \rightarrow qW) = 0.99 \pm 0.29$. In the three-generation SM, B_b is related to CKM matrix elements as

$$B_b \equiv \frac{|V_{tb}|^2}{|V_{tb}|^2 + |V_{ts}|^2 + |V_{td}|^2}. \quad (12)$$

Three-generation unitarity dictates that the denominator of (12) is 1.0, so that the measurement of B_b implies⁴⁴ $|V_{tb}| > 0.76$ at 95% c.l. However, within the 3-generation SM, data on the light quarks combined with CKM unitarity has already provided¹² the much tighter constraints $0.9991 < |V_{tb}| < 0.9994$.

If we add a fourth generation of quarks, the analysis differs. A search by DØ has constrained¹² any 4-th generation b' quark to have a mass greater than $m_t - m_W$, so that the top quark could not readily decay to b' . This means that the original expression (12) for B_b is still valid. However, once there are four generations, the denominator of the RHS of (12) need not equal 1.0. Then the CDF measurement of B_b implies $|V_{tb}| \gg |V_{td}|, |V_{ts}|$. In contrast, light-quark data combined with 4-generation CKM unitarity allows $|V_{tb}|$ to lie in the range¹² $0.05 < |V_{tb}| < 0.9994$. While the measurement of B_b gives only qualitative information about $|V_{tb}|$, that information is new and useful in the context of a 4-generation model.

Direct measurement of $|V_{tb}|$ in single top-quark production (via $q\bar{q} \rightarrow W^* \rightarrow t\bar{b}$ and $gW \rightarrow t\bar{b}$) at the Tevatron should reach an accuracy³¹ of 10% in Run IIa (5% in Run IIb).

FCNC decays

CDF has set limits⁴⁵ on the flavor-changing decays $t \rightarrow Zq, \gamma q$ which are GIM-suppressed in the SM. In seeking $t \rightarrow Zq$ they looked at $p\bar{p} \rightarrow t\bar{t} \rightarrow qZbW, qZbZ \rightarrow \ell\ell + 4$ jets with high jet E_T . The SM background from WW, ZZ and WZ events is predicted to be 0.6 ± 0.2 events. The data contains a single candidate (in which the Z decayed to muons). On this basis, the 95% c.l. upper limit $B(t \rightarrow Zq) < 0.33$ was set. To study $t \rightarrow \gamma q$, CDF examined $p\bar{p} \rightarrow t\bar{t} \rightarrow Wb\gamma q$ events. If the W decayed leptonically, the signature was $\gamma + \ell + E_{\cancel{T}} + (\geq 2)$ jets; if hadronically, the signature was $\gamma + (\geq 4)$ jets with one jet b -tagged. The expected SM background is a single event. Finding a single candidate event (with a leptonic W decay), CDF set the 95% c.l. upper bound $B(t \rightarrow \gamma q) < 0.032$. Run II will provide much greater sensitivity to these decays,³¹ as indicated in Table 3.

Table 3. Run II sensitivity³¹ to FCNC top decays as a function of $\int \mathcal{L} dt$.

	1 fb ⁻¹	10 fb ⁻¹	100 fb ⁻¹
$BR(t \rightarrow Zq)$	0.015	3.8×10^{-3}	6.3×10^{-4}
$BR(t \rightarrow \gamma q)$	3.0×10^{-3}	4.0×10^{-4}	8.4×10^{-5}

1.7 Summary

The Run I experiments at the Tevatron discovered the top quark and provided the first measurements of a variety of properties including m_t , Γ_t , σ_{tt} , $\frac{d\sigma}{dM_{tt}}$, $\frac{d\sigma}{dp_T}$, κ , σ_{tb} , \mathcal{F}_0 , \mathcal{F}_+ , B_b , $\Gamma(t \rightarrow Zq)$, and $\Gamma(t \rightarrow \gamma q)$. As we have seen, most of the measurements were limited in precision by the small top sample size. This will be ameliorated at Run II and future colliders.

As a starting point for further discussion, we note that each property measured has been seen to have multiple implications for theory. Moreover, the interpretation of the measurement can depend critically on the theoretical context. In some cases, measurements may even shed more light on the merits of proposed non-standard physics than on the Standard Model itself. This is the line of thought we shall take up in the second section of the talk.

2 Beyond the Standard Model

Two central concerns of particle theory are finding the cause of electroweak symmetry breaking and identifying the origin of flavor symmetry breaking by which the quarks and leptons obtain their diverse masses. The Standard Higgs Model of particle physics, based on the gauge group $SU(3)_c \times SU(2)_W \times U(1)_Y$ accommodates both symmetry breakings by including a fundamental weak doublet of scalar (“Higgs”) bosons $\phi = \begin{pmatrix} \phi^+ \\ \phi^0 \end{pmatrix}$ with potential function $V(\phi) = \lambda \left(\phi^\dagger \phi - \frac{1}{2}v^2 \right)^2$. However the SM does not explain the dynamics responsible for the generation of mass. Furthermore, the scalar sector suffers from two serious problems. The scalar mass is unnaturally sensitive to the presence of physics at any higher scale Λ (e.g. the Planck scale), as shown in Figure 17. This is known as the gauge hierarchy problem. In addition, if the scalar must provide a good description of physics up to arbitrarily high scale (i.e., be fundamental), the scalar’s self-coupling (λ) is driven to zero at finite energy scales as indicated in Figure 17. That is, the scalar field theory is free (or “trivial”). Then the scalar cannot fill its intended role: if $\lambda = 0$, the electroweak symmetry is not spontaneously broken. The scalars involved



Figure 17. (left) Naturalness problem: $M_H^2 \propto \Lambda^2$. (right) Triviality: $\beta(\lambda) = \frac{3\lambda^2}{2\pi^2} > 0$.



Figure 18. $\delta M_H^2 \sim \frac{g_f^2}{4\pi^2}(m_f^2 - m_s^2) + m_s^2 \log \Lambda^2$

in electroweak symmetry breaking must therefore be a party to new physics at some finite energy scale – e.g., they may be composite or may be part of a larger theory with a UV fixed point. The SM is merely a low-energy effective field theory, and the dynamics responsible for generating mass must lie in physics outside the SM.

One interesting possibility is to introduce supersymmetry.⁴⁶ The gauge structure of the minimal supersymmetric SM (MSSM) is identical to that of the SM, but each ordinary fermion (boson) is paired with a new boson (fermion) called its “superpartner” and two Higgs doublets are needed to provide mass to all the ordinary fermions. As sketched in Figure 18, each loop of ordinary particles contributing to the Higgs boson’s mass is countered by a loop of superpartners. If the masses of the ordinary particles and superpartners are close enough, the gauge hierarchy can be stabilized.⁴⁷ Supersymmetry relates the scalar self-coupling to gauge couplings, so that triviality is not a concern.

Another intriguing idea, dynamical electroweak symmetry breaking,⁴⁸ is that the scalar states involved in electroweak symmetry breaking could be manifestly composite at scales not much above the electroweak scale $v \sim 250$ GeV. In these theories, a new strong gauge interaction with $\beta < 0$ (e.g., technicolor) breaks the chiral symmetries of massless fermions f at a scale $\Lambda \sim 1$ TeV. If the fermions carry appropriate electroweak quantum numbers (e.g. LH weak doublets and RH weak singlets), the resulting condensate $\langle \bar{f}_L f_R \rangle \neq 0$ breaks the electroweak symmetry as desired. The Goldstone Bosons (technipions) of the chiral symmetry breaking simply become the longitudinal modes of the W and Z . The logarithmic running of the strong gauge coupling renders the low value of the electroweak scale (i.e. the gauge hierarchy) natural.

The absence of fundamental scalars obviates concerns about triviality.

Once we are willing to consider physics outside the SM, seeking experimental evidence is imperative. One logical place to look is in the properties of the most recently discovered state, the top quark. The fact that $m_t \sim v_{weak}$ suggests that the top quark may afford us insight about non-standard models of electroweak physics and could even play a special role in electroweak and flavor symmetry breaking. Since the sample of top quarks accumulated in Tevatron Run I was small, many of the top quark's properties are still only loosely constrained. The top quark may yet prove to have properties that set it apart from the other quarks, such as light related states, low-scale compositeness, or unusual gauge couplings.

The Run II experiments will help us evaluate these ideas. One approach would be to classify measurable departures from SM predictions and identify the theories which could produce them.⁴⁹ For example, an unexpectedly large rate for $t\bar{t}$ production could signal the presence of a coloron resonance, a techni-eta decaying to $t\bar{t}$ or a gluino decaying to $t\bar{t}$. The approach we adopt here, is to consider general classes of theoretical models and identify signals characteristic of each. We will discuss two-higgs and SUSY models, dynamical symmetry breaking, new gauge interactions for the top quark and the phenomenology of strong top dynamics.

2.1 Multiple-Scalar-Doublet Models

Many quite different kinds of models include relatively light charged scalar bosons, into which top may decay: $t \rightarrow H^+b$. The general class of models that includes multiple Higgs bosons⁵⁰ features charged scalars that can be light. Dynamical symmetry breaking models with more than the minimal two flavors of new fermions (e.g. technicolor with more than one weak doublet of technifermions) typically possess pseudoGoldstone boson states, some of which can couple to third generation fermions. SUSY models must include at least two Higgs doublets in order to provide mass to both the up and down quarks, and therefore have a charged scalar in the low-energy spectrum.

Experimental limits on charged scalars are often phrased in the language of a two-higgs-doublet model. In addition to the usual input parameters α_{em} , G_F and M_Z required to specify the electroweak sector of the SM, two additional quantities are relevant for the process $t \rightarrow H^+b$: $\tan\beta$ (the ratio of the vev's of the two scalar doublets) and M_{H^\pm} .

If the mass of the charged scalar is less than $m_t - m_b$, then the decay $t \rightarrow H^+b$ can compete with the standard top decay mode $t \rightarrow Wb$. Since the

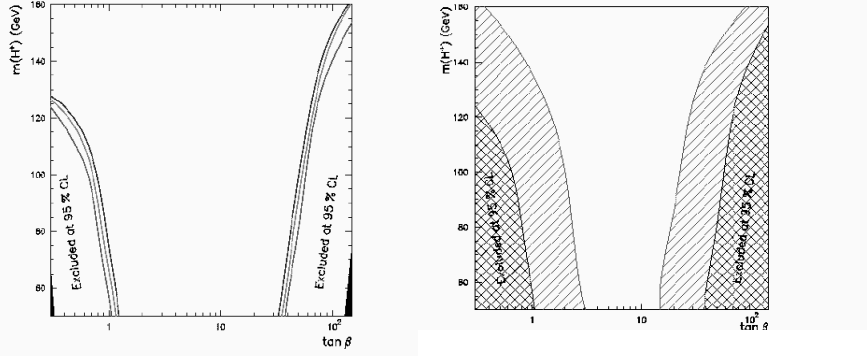


Figure 19. DØ charged scalar searches⁵¹ in $t \rightarrow H^\pm b$. (left) Run I limits for $m_t = 175$ GeV. The region below the top (middle, bottom) contours is excluded if $\sigma(t\bar{t}) = 4.5, 5.0, 5.5$ pb. (right) Projected Run II reach⁵² assuming $\sqrt{s} = 2$ TeV, $\int \mathcal{L} dt = 2\text{fb}^{-1}$, and $\sigma(t\bar{t}) = 7\text{pb}$.

tbH^\pm coupling depends on $\tan\beta$ as⁵⁰

$$g_{tbH^+} \propto m_t \cot\beta(1 + \gamma_5) + m_b \tan\beta(1 - \gamma_5) , \quad (13)$$

the additional decay mode is significant for either large or small values of $\tan\beta$. The charged scalar, in turn, decays as $H^\pm \rightarrow cs$ or $H^\pm \rightarrow t^*b \rightarrow Wbb$ if $\tan\beta$ is small and as $H^\pm \rightarrow \tau\nu_\tau$ if $\tan\beta$ is large. In either case, the final state reached through an intermediate H^\pm will cause the original $t\bar{t}$ event to fail the usual cuts for the lepton + jets channel. A reduced rate in this channel can therefore signal the presence of a light charged scalar. As shown in Figure 19, DØ has set a limit⁵¹ on M_{H^\pm} as a function of $\tan\beta$ and $\sigma_{t\bar{t}}$. In Run II the limits should span a wider range of $\tan\beta$ and reach nearly to the kinematic limit.

2.2 SUSY Models

The heavy top quark plays a role in several interesting issues related to Higgs and sfermion masses in supersymmetric models.

Scalar mass-squared

SUSY models need to explain why the scalar Higgs boson acquires a negative mass-squared (breaking the electroweak symmetry) while the scalar

fermions do not (preserving color and electromagnetism). In a number of SUSY models, such as the MSSM with GUT unification or models with dynamical SUSY breaking, the answer involves the heavy top quark.⁴⁶ In these theories, the masses of the Higgs bosons and sfermions are related at a high energy scale M_X :

$$M_{h,H}^2(M_X) = m_0^2 + \mu^2 \quad M_{\tilde{f}}^2(M_X) = m_0^2 \quad (14)$$

where the squared masses are all positive so that the vacuum preserves the color and electroweak symmetries. To find the masses of the scalar particles at lower energy scales, one studies the renormalization group running of the masses.⁵³ The large mass of the top quark makes significant corrections to the running masses. Comparing the evolution equations⁵⁴ for the Higgs, the scalar partner of t_R and the scalar partner of $Q_L \equiv (t, b)_L$,

$$\frac{d}{d \ln(q)} \begin{pmatrix} M_h^2 \\ \tilde{M}_{t_R}^2 \\ \tilde{M}_{Q_L}^2 \end{pmatrix} = -\frac{8\alpha_s}{3\pi} M_3^2 \begin{pmatrix} 0 \\ 1 \\ 1 \end{pmatrix} + \frac{\lambda_t^2}{8\pi^2} (\tilde{M}_{Q_L}^2 + \tilde{M}_{t_R}^2 + M_h^2 + A_{o,t}^2) \begin{pmatrix} 3 \\ 2 \\ 1 \end{pmatrix} \quad (15)$$

it is clear that the influence of the top quark Yukawa coupling is greatest for the Higgs. At scale q , the approximate solution for M_h is

$$M_h^2(q) = M_h^2(M_X) - \frac{3}{8\pi^2} \lambda_t^2 (\tilde{M}_{Q_L}^2 + \tilde{M}_{t_R}^2 + M_h^2 + A_{o,t}^2) \ln \left(\frac{M_X}{q} \right) \quad (16)$$

and λ_t is seen to be reducing M_h^2 . For $m_t \sim 175$ GeV, this effect drives the Higgs mass, and only the Higgs mass, negative – just as desired.⁵⁵

Light Higgs mass

The low-energy spectrum of the MSSM includes a pair of neutral scalars h^0 (by convention, the lighter one) and H^0 . At tree level, $M_h < M_Z |\cos(2\beta)|$ where $\tan \beta$ is the ratio of the vev's of the two Higgs doublets.⁵⁰ Searches for light Higgs bosons then appear to put low values of $\tan \beta$ in jeopardy. In fact experiment has now pushed the lower bound on M_h well above the Z mass: $M_h \gtrsim 107.7$ GeV.¹⁴

Enter the top quark. Radiative corrections to M_h involving virtual top quarks introduce a dependence on the top mass. For large m_t , this can raise the upper bound on M_h significantly.⁵⁶ When $\tan \beta > 1$,

$$M_h^2 < M_Z^2 \cos^2(2\beta) + \frac{3G_f}{\sqrt{2}\pi^2} m_t^4 \ln \left(\frac{\tilde{m}^2}{m_t^2} \right) \quad (17)$$

and the m_t^4 term raises the upper bound well above M_Z . Including higher-order corrections, the most general limit⁵⁶ appears to be $M_h < 130$ GeV, well above the current bounds but in reach of upcoming experiment.

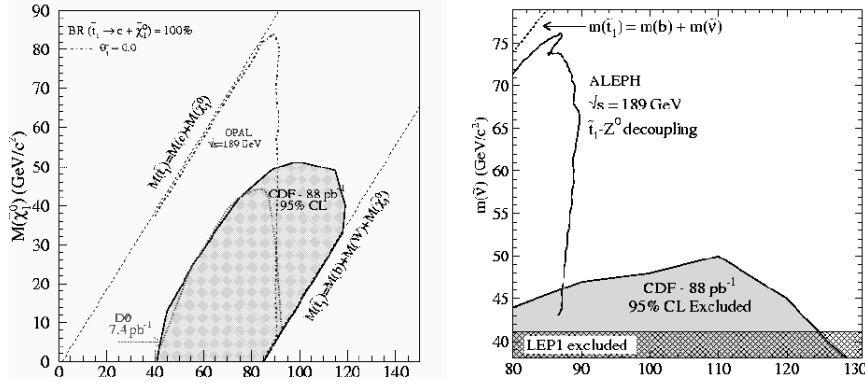


Figure 20. Limits⁵⁷ on Light Stop (left) via $\tilde{t}_1 \rightarrow c\tilde{\chi}_1^0$. (right) via $\tilde{t}_1 \rightarrow b\tilde{\chi}_1^+ \rightarrow b\ell\tilde{\nu}$ or direct $\tilde{t}_1 \rightarrow b\ell\tilde{\nu}$ assuming equal branching to all lepton flavors.

Light top squarks

Since SUSY models include a bosonic partner for each SM fermion, there is a pair of complex scalar top squarks affiliated with the top quark (one for t_L , one for t_R). A look at the mass-squared matrix for the stops⁴⁶ (in the \tilde{t}_L, \tilde{t}_R basis)

$$\tilde{m}_t^2 = \begin{pmatrix} \tilde{M}_Q^2 + m_t^2 & m_t(A_t + \mu \cot \beta) \\ +M_Z^2(\frac{1}{2} - \frac{2}{3}\sin^2 \theta_W) \cos 2\beta & \\ m_t(A_t + \mu \cot \beta) & \tilde{M}_U^2 + m_t^2 \\ & +\frac{2}{3}M_Z^2 \sin^2 \theta_W \cos 2\beta \end{pmatrix} \quad (18)$$

reveals that the off-diagonal entries are proportional to m_t . Hence, a large m_t can drive one of the top squark mass eigenstates to be relatively light. Experiment still allows a light stop,⁵⁷ as may be seen in Figure 20; Run II will be sensitive to higher stop masses in several decay channels⁵⁸ (Figure 21).

Perhaps some of the Run I “top” sample included top squarks.⁵⁹ If the top squark is not much heavier than the top quark, it is possible that $\tilde{t}\tilde{t}$ production occurred in Run I, with the top squarks subsequently decaying to top plus neutralino or gluino (depending on the masses of the gauginos). If the top is a bit heavier than the stop, some top quarks produced in $t\bar{t}$ pairs in Run I may have decayed to top squarks via $t \rightarrow \tilde{t}\tilde{N}$ with the top squarks’ subsequent decay being either semi-leptonic $\tilde{t} \rightarrow b\ell\tilde{\nu}$ or flavor-changing $\tilde{t} \rightarrow c\tilde{N}, c\tilde{g}$. With

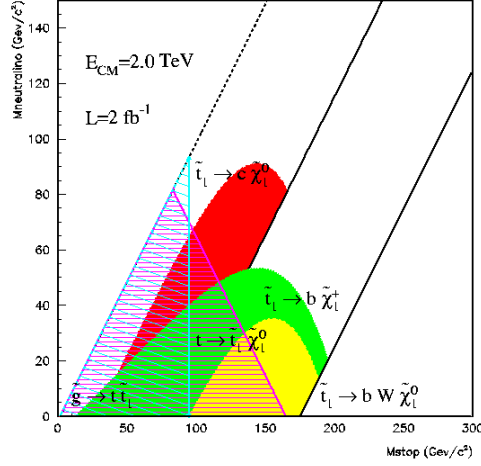


Figure 21. Anticipated Run II Stop limits from various decay channels.⁵⁸

either ordering of mass, it is possible that gluino pair production occurred, followed by $\tilde{g} \rightarrow t\bar{t}$. These ideas can be tested using the rate, decay channels, and kinematics of top quark events.⁴⁹ For example, stop or gluino production could increase the apparent $t\bar{t}$ production rate above that of the SM. Or final states including like-sign dileptons could result from gluino decays.

2.3 Dynamical Electroweak Symmetry Breaking

Extended technicolor (ETC) is an explicit realization of dynamical electroweak symmetry breaking and fermion mass generation.⁴⁸ One starts with a strong gauge group (technicolor) felt only by a set of new massless fermions (technifermions) and extends the technicolor gauge group to a larger (ETC) group under which ordinary fermions are also charged. At a scale M , ETC breaks to its technicolor subgroup and the gauge bosons coupling ordinary fermions to technifermions acquire a mass of order M . At a scale $\Lambda_{TC} < M$, a technifermion condensate breaks the electroweak symmetry as described earlier. The quarks and leptons acquire mass because massive ETC gauge bosons couple them to the condensate. The top quark's mass, e.g., arises when the condensing technifermions transform the scattering diagram in Figure 22 (left) into the top self-energy diagram shown at right. Its size is

$$m_t \approx (g_{ETC}^2/M^2)\langle T\bar{T} \rangle \approx (g_{ETC}^2/M^2)(4\pi v^3) \quad . \quad (19)$$



Figure 22. (left) Top-technifermion scattering mediated by a heavy ETC gauge boson. (right) Technifermion condensation creates the top quark mass.

Thus M must satisfy $M/g_{ETC} \approx 1.4$ TeV in order to produce $m_t = 175$ GeV.

While this mechanism works well in principle, it is difficult to construct a complete model that can accommodate a large value for m_t while remaining consistent with precision electroweak data. Two key challenges have led model-building in new and promising directions. First, the dynamics responsible for the large value of m_t must couple to b_L because t and b are weak partners. How, then, can one obtain a predicted value of R_b that agrees with experiment? Attempts to answer this question have led to models in which the weak interactions of the top quark^{60,64} (and, perhaps, all third generation fermions) are non-standard. Second, despite the large mass splitting $m_t \gg m_b$, the value of the rho parameter is very near unity. How can dynamical models accommodate large weak isospin violation in the $t - b$ sector without producing a large shift in M_W ? This issue has sparked theories in which the strong (color) interactions of the top quark⁶¹ (and possibly other quarks⁶²) are modified from the predictions of QCD.

In the remainder of this talk, we explore the theoretical and experimental implications of having non-standard gauge interactions for the top quark.

2.4 New Top Weak Interactions

In classic ETC models, the large value of m_t comes from ETC dynamics at a relatively low scale M of order a few TeV. At that scale, the weak symmetry is still intact so that t_L and b_L function as weak partners. Moreover, experiment tells us that $|V_{tb}| \approx 1$. As a result, the ETC dynamics responsible for generating m_t must couple with equal strength to t_L and b_L . While many properties of the top quark are only loosely constrained by experiment, the b quark has been far more closely studied. In particular, the LEP measurements of the $Zb\bar{b}$ coupling are precise enough to be sensitive to the quantum corrections arising from physics beyond the SM. As we now discuss, radiative corrections to the $Zb\bar{b}$ vertex from low-scale ETC dynamics can be so large that new weak interactions for the top quark are required to make the models consistent with experiment.^{63,60}



Figure 23. Fermion currents coupling to the weak-singlet ETC boson that generates m_t .

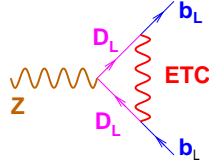


Figure 24. Direct correction to the $Zb\bar{b}$ vertex from the ETC gauge boson responsible for m_t in a commuting model.

To begin, consider the usual ETC models in which the extended technicolor and weak gauge groups commute, so that the ETC gauge bosons carry no weak charge. In these models, the ETC gauge boson whose exchange gives rise to m_t couples to the fermion currents⁶³

$$\xi (\bar{\psi}_L^i \gamma^\mu T_L^{ik}) + \xi^{-1} (\bar{t}_R \gamma^\mu U_R^k) \quad (20)$$

where ξ is a Clebsch of order 1 (see Figure 23). Then the top quark mass arises from technifermion condensation and ETC boson exchange as in Figure 22, with the relevant technifermions being U_L and U_R .

Exchange of the same⁶³ ETC boson causes a direct (vertex) correction to the $Z \rightarrow b\bar{b}$ decay as shown in Figure 24; note that it is D_L technifermions with $I_3 = -\frac{1}{2}$ which enter the loop. This effect reduces the magnitude of the $Zb\bar{b}$ coupling by

$$\delta g_L = \frac{e}{4 \sin \theta \cos \theta} \left(\frac{g^2 v^2}{M^2} \right) \quad (21)$$

Given the relationship between M and m_t from Eq. 19, we find

$$\frac{g^2 v^2}{M^2} \approx \frac{m_t}{4\pi v} \quad (22)$$

so that the top quark mass sets the size of the coupling shift.

How to observe the shift in the couplings? The vertex correction will certainly produce a correction $\delta\Gamma_b$ to the Z decay width $\Gamma(Z \rightarrow b\bar{b})$. But since

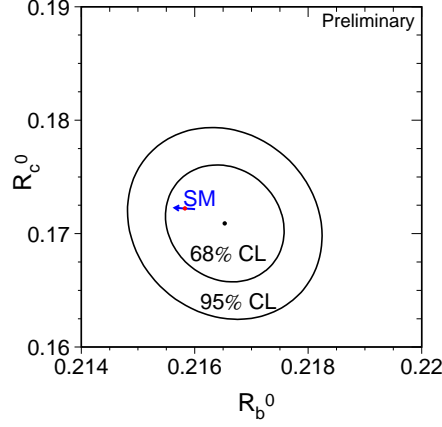


Figure 25. Data¹⁴ on R_b and R_c showing experimental best fit (dot) and SM prediction (arrow). A 5% negative shift in R_b is clearly excluded.

Γ_b also receives oblique radiative corrections, $\Gamma_b^{corr.} = (1 + \Delta\rho)(\Gamma_b + \delta\Gamma_b)$, a measurement of Γ_b is not the best way to track δg_b . The ratio of Γ_b to the hadronic decay width of the Z

$$R_b \equiv \Gamma(Z \rightarrow b\bar{b})/\Gamma(Z \rightarrow \text{hadrons}) \quad (23)$$

is also proportional to δg_L and has the additional advantage that oblique and QCD radiative corrections each cancel in the ratio (up to factors suppressed by small quark masses). One finds⁶³

$$\frac{\delta R_b}{R_b} \approx -5.1\% \cdot \xi^2 \cdot \left(\frac{m_t}{175\text{GeV}} \right) \quad (24)$$

Such a large shift in R_b is excluded¹⁴ by the data (see Figure 25). Then the ETC models whose dynamics produces this shift are likewise excluded.

This suggests one should consider an alternative class of ETC models⁶⁰ in which the weak group $SU(2)_W$ is embedded in G_{ETC} , so that the weak bosons carry weak charge. Embedding the weak interactions of all quarks in a low-scale ETC group would produce masses of order m_t for all up-type quarks. Instead, one can extend $SU(2)$ to a direct product group $SU(2)_h \times SU(2)_\ell$ such that the third generation fermions transform under $SU(2)_h$ and the others under $SU(2)_\ell$. Only $SU(2)_h$ is embedded in the low-scale ETC group; the masses of the light fermions will come from physics at higher scales. Breaking

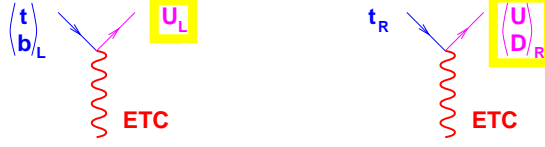


Figure 26. Fermion currents coupling to the weak-doublet ETC boson that generates m_t in non-commuting ETC models.

the two weak groups to their diagonal subgroup ensures approximate Cabibbo universality at low energies. The electroweak and technicolor gauge structure of these non-commuting models is sketched below⁶⁰:

$$\begin{aligned}
& G_{ETC} \times SU(2)_{light} \times U(1) \\
& \quad \downarrow f \\
& G_{TC} \times SU(2)_{heavy} \times SU(2)_{light} \times U(1)_Y \\
& \quad \downarrow u \\
& G_{TC} \times SU(2)_{weak} \times U(1)_Y \\
& \quad \downarrow v \\
& G_{TC} \times U(1)_{EM}
\end{aligned} \tag{25}$$

Due to the extended gauge structure, there are now two non-standard contributions to R_b , one from the dynamics that generates m_t and the other from the mixing of the two Z bosons from the two weak groups. The ETC boson responsible for m_t now couples weak-double fermions to weak-singlet technifermions (and vice versa) as in Figure 26. The radiative correction to the $Zb\bar{b}$ vertex is as in Figure 24 except that the technifermions involved are now U_L with $T_3 = +\frac{1}{2}$. As a result, the shift in δg_L and R_b have the same size the results in Eqs. 21 and 24 – but the opposite sign.⁶⁰ Were these the only contributions to R_b , this class of models would be excluded.

Consider, however, what happens when the $SU(2)_h \times SU(2)_\ell \times U(1)_Y$ bosons mix to form mass eigenstates.⁶⁰ The result is heavy states W^H, Z^H that couple mainly to the third generation, light states W^L, Z^L resembling the standard W and Z , and a massless photon $A^\mu = \sin \theta [\sin \phi W_{3\ell}^\mu + \cos \phi W_{3h}^\mu] + \cos \theta X^\mu$ coupling to $Q = T_{3h} + T_{3\ell} + Y$. Here, ϕ describes the mixing between the two weak groups and θ is the usual weak angle. In terms of a rotated basis (with $s \equiv \sin \phi$, $c \equiv \cos \phi$)

$$W_1^\pm = s W_\ell^\pm + c W_h^\pm \quad W_2^\pm = c W_\ell^\pm - s W_h^\pm$$

$$\begin{aligned}
D^\mu &= \partial^\mu + ig (T_\ell^\pm + T_h^\pm) W_1^{\pm\mu} + ig \left(\frac{c}{s} T_\ell^\pm - \frac{s}{c} T_h^\pm \right) W_2^{\pm\mu} \\
Z_1 &= \cos\theta (s W_{3\ell} + c W_{3h}) - \sin\theta X \quad Z_2 = c W_{3\ell} - s W_{3h} \\
D^\mu &= \partial^\mu + i \frac{g}{\cos\theta} (T_{3\ell} + T_{3h} - \sin^2\theta Q) Z_1^\mu
\end{aligned} \tag{26}$$

where W_1, Z_1 have SM couplings and all non-standard couplings accrue to W_2, Z_2 , the mass eigenstates are (with $x \equiv u^2/v^2$)

$$\begin{aligned}
W^L &\approx W_1 - \frac{c^3 s}{x} W_2, \quad W^H \approx W_2 + \frac{c^3 s}{x} W_1 \\
Z^L &\approx Z_1 - \frac{c^3 s}{x \cos\theta} Z_2, \quad Z^H \approx Z_2 + \frac{c^3 s}{x \cos\theta} Z_1
\end{aligned} \tag{27}$$

and the heavy boson masses are degenerate: $M_{W^H} \approx M_{Z^H} \approx M_W \sqrt{x}/sc$. The Z^L coupling to quarks thus differs from the SM value by $\delta g_L = (c^4/x)T_{3\ell} - (c^2 s^2/x)T_{3h}$ which reduces R_b by⁶⁰

$$\frac{\delta R_b}{R_b} \approx -5.1\% [\sin^2\phi \frac{f^2}{u^2}] \tag{28}$$

where the term in square brackets is $\mathcal{O}(1)$.

As the ETC and ZZ' mixing contributions to R_b are of the same magnitude, but opposite size, R_b can be consistent with experiment in non-commuting ETC models. The key element that permits a large m_t and a small value of R_b to co-exist is the presence of non-standard weak interactions for the top quark.⁶⁰ This is something experiment can test, and has since been incorporated into models such as topflavor⁶⁴ and top seesaw.⁶⁵

There are several ways to test whether the high-energy weak interactions have the form $SU(2)_h \times SU(2)_\ell$. One possibility is to search for the extra weak bosons. The bosons' predicted effects on precision electroweak data gives rise to the exclusion curve⁶⁶ in Figure 27. Low-energy exchange of Z^H and W^H bosons would cause apparent four-fermion contact interactions; LEP limits on $eebb$ and $ee\tau\tau$ contact terms imply⁶⁷ $M_{Z^H} \gtrsim 400$ GeV. Direct production of Z^H and W^H at Fermilab is also feasible; a Run II search for $Z^H \rightarrow \tau\tau \rightarrow e\mu X$ will be sensitive⁶⁷ to Z^H masses up to 750 GeV. Another possibility is to measure the top quark's weak interactions in single top production. Run II should measure the ratio of single top and single lepton cross-sections $R_\sigma \equiv \sigma_{tb}/\sigma_{\ell\nu}$ to $\pm 8\%$ in the W^* process.⁶⁸ A number of systematic uncertainties, such as those from parton distribution functions, cancel in the ratio. In the SM, R_σ is proportional to the square of the Wtb coupling. Non-commuting ETC models affect the ratio in two ways: mixing of the W_h and W_ℓ alters the W^L coupling to fermions, and both W^L and W^H exchange contributes to the

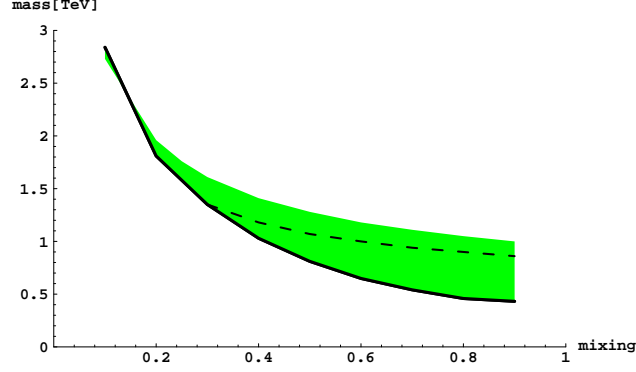


Figure 27. FNAL Run II single top production can explore the shaded region of the $M_{W'}$ vs. $\sin^2 \phi$ plane.⁶⁹ The area below the solid curve is excluded by precision electroweak data.⁶⁶ In the shaded region R_σ increases by $\geq 16\%$; below the dashed curve, by $\geq 24\%$.

$$\begin{array}{c} \text{wavy line} \\ \mathbf{W}_i \end{array} \text{---} \text{circle} \text{---} \begin{array}{c} \text{wavy line} \\ \mathbf{W}_i \end{array} = i\Pi_{ii}g^{\mu\nu} + \dots$$

Figure 28. Electroweak boson propagator used in calculation of $\Delta\rho$.

cross-sections^d. Computing the shift in R_σ from these effects reveals (Figure 27) that Run II will be sensitive⁶⁹ to W^H bosons up to masses of about 1.5 TeV.

2.5 New Top Strong Interactions

At tree-level in the SM, $\rho \equiv M_W^2/M_Z^2 \cos^2 \theta_W \equiv 1$ due to a “custodial” global $SU(2)$ symmetry relating members of a weak isodoublet. Because the two fermions in each isodoublet have different masses and hypercharges, however, oblique⁷⁰ radiative corrections to the W and Z propagators alter the value of ρ . The one-loop correction from the (t,b) doublet is particularly large because $m_t \gg m_b$. The shift in ρ is computed from the propagators in Figure 28 as⁷⁰

$$\Delta\rho(0) \equiv \rho(0) - 1 = \frac{e^2}{\sin^2 \theta_W \cos^2 \theta_W M_Z^2} [\Pi_{11}(0) - \Pi_{33}(0)] \quad (29)$$

^dThe ETC dynamics which generates m_t has no effect on the Wtb vertex because the relevant ETC boson does not couple to b_R .

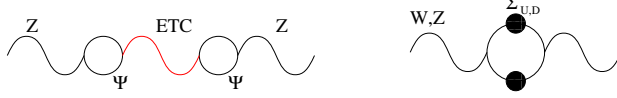


Figure 29. ETC contributions to $\Delta\rho$: (left) direct, from gauge boson mixing (right) indirect, from technifermion mass splitting.

Experiment¹² finds $|\Delta\rho| \leq 0.4\%$, a stringent constraint on isospin-violating new physics. For example, a heavy lepton doublet (N,E) with standard weak couplings and mass $\gg M_Z$ would add⁷⁰

$$\Delta\rho_{N,E} \approx \frac{\alpha_{EM}}{16\pi \sin^2 \theta_W \cos^2 \theta_W M_Z^2} [m_N^2 + m_E^2 - \frac{2m_N^2 m_E^2}{m_N^2 - m_E^2} \log(\frac{m_N^2}{m_E^2})] \quad (30)$$

and a new quark doublet, three times as much; the data forces the new fermions to be nearly degenerate.

Dynamical theories of mass generation like ETC must break weak isospin in order to produce the large top-bottom mass splitting. However, the new dynamics may also cause large contributions to $\delta\rho$. Direct mixing between and ETC gauge boson and the Z (Figure 29) induces the dangerous effect⁷¹

$$\Delta\rho \approx 12\% \cdot \left(\frac{\sqrt{N_D} F_{TC}}{250 \text{ GeV}} \right)^2 \cdot \left(\frac{1 \text{ TeV}}{M_{ETC}/g_{ETC}} \right)^2 \quad (31)$$

in models with N_D technifermion doublets and technipion decay constant F_{TC} . To avoid this, one could make the ETC boson heavy; however the required $M_{ETC}/g_{ETC} > 5.5 \text{ TeV} (\sqrt{N_D} F_{TC}/250 \text{ GeV})$ is too large to produce $m_t = 175 \text{ GeV}$. Instead, one must obtain $N_D F_{TC}^2 \ll (250 \text{ GeV})^2$ by separating the ETC sectors responsible for electroweak symmetry breaking and the top mass. A second contribution comes indirectly⁷² through the technifermion mass splitting: $\Delta\rho \sim (\Sigma_U(0) - \Sigma_D(0))^2/M_Z^2$, as in Figure 29. Again, a cure^{61,73} is to arrange for the t and b to get only part of their mass from technicolor. As sketched in Figure 30, suppose M_{ETC} is large and ETC makes only a small contribution to the fermion and technifermion masses. At a scale between M_{ETC} and Λ_{TC} new strong dynamics felt only by (t,b) turns on and generates $m_t \gg m_b$. The technifermion mass splitting is small, $\Delta\Sigma(0) \approx m_t(M_{ETC} - m_b(M_{ETC})) \ll m_t$, and no large contributions to $\Delta\rho$ ensue.

The realization that new strongly-coupled dynamics for the (t,b) doublet could be so useful has had a dramatic effect on model-building. Models in which some (topcolor⁶¹) or even all (top mode,⁷⁴ top seesaw⁷⁵) of electroweak

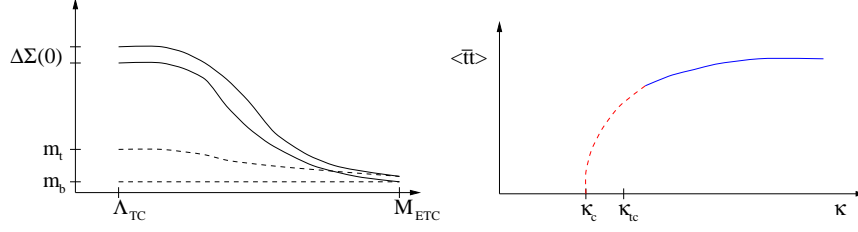


Figure 30. (left) ETC and new top dynamics generate masses for technifermions, t and b . (right) Second-order phase transition forms a top condensate for $\kappa > \kappa_c$.

symmetry breaking is due to a top condensate have proliferated. One physical realization of a new interaction for the top is a spontaneously broken extended gauge group called topcolor⁶¹: $SU(3)_h \times SU(3)_\ell \rightarrow SU(3)_{QCD}$. The (t,b) doublet transforms under $SU(3)_h$ and the light quarks, under $SU(3)_\ell$. Below the symmetry-breaking scale M , the spectrum includes massive topgluons which mediate vectorial color-octet interactions among top quarks: $-(4\pi\kappa/M^2)(\bar{t}\gamma_\mu \frac{\lambda^a}{2}t)^2$. If the coupling κ lies above a critical value ($\kappa_c = 3\pi/8$ in the NJL⁷⁶ approximation), a top condensate forms (Figure 30). For a second-order phase transition, $\langle \bar{t}t \rangle/M^3 \propto (\kappa - \kappa_c)/\kappa_c$, so the top quark mass generated by this dynamics can lie well below the symmetry breaking scale; so long as M is not too large, the scale separation need not imply an unacceptable degree of fine tuning.

A more complete model incorporating these ideas is topcolor-assisted technicolor⁶¹ (TC2). The symmetry-breaking structure is:

$$\begin{aligned}
& G_{TC} \times SU(3)_h \times SU(3)_\ell \times SU(2)_W \times U(1)_h \times U(1)_\ell \\
& \quad \downarrow \quad M \gtrsim 1 \text{ TeV} \\
& G_{TC} \times SU(3)_{QCD} \times SU(2)_W \times U(1)_Y \\
& \quad \downarrow \quad \Lambda_{TC} \sim 1 \text{ TeV} \\
& G_{TC} \times SU(3)_{QCD} \times U(1)_{EM}
\end{aligned} \tag{32}$$

Below the scale M , the heavy topgluons and Z' mediate new effective interactions^{61,77} for the (t,b) doublet

$$-\frac{4\pi\kappa_3}{M^2} \left[\bar{\psi} \gamma_\mu \frac{\lambda^a}{2} \psi \right]^2 - \frac{4\pi\kappa_1}{M^2} \left[\frac{1}{3} \bar{\psi}_L \gamma_\mu \psi_L + \frac{4}{3} \bar{t}_R \gamma_\mu t_R - \frac{2}{3} \bar{b}_R \gamma_\mu b_R \right]^2 \tag{33}$$

where the λ^a are color matrices and $g_{3h} \gg g_{3\ell}$, $g_{1h} \gg g_{1\ell}$. The κ_3 terms are uniformly attractive; were they alone, they would generate large m_t **and** m_b .

The κ_1 terms, in contrast, include a repulsive component for b . As a result, the combined effective interactions^{61,77}

$$\kappa^t = \kappa_3 + \frac{1}{3}\kappa_1 > \kappa_c > \kappa_3 - \frac{1}{6}\kappa_1 = \kappa^b \quad (34)$$

can be super-critical for top, causing $\langle \bar{t}t \rangle \neq 0$ and a large m_t , and sub-critical for bottom, leaving $\langle \bar{b}b \rangle = 0$.

The benefits of including new strong dynamics for the top quark are clear in TC2 models.⁷⁷ Because technicolor is responsible for most of electroweak symmetry breaking, $\Delta\rho \approx 0$. Direct contributions to $\Delta\rho$ are avoided because the top condensate provides only $f \sim 60$ GeV; indirect contributions are not an issue if the technifermion hypercharges preserve weak isospin. The top condensate yields a large top mass. ETC dynamics at $M_{ETC} \gg 1$ TeV generate the light m_f without large FCNC and contribute only ~ 1 GeV to the heavy quark masses so there is no large shift in R_b .

2.6 Phenomenology of Strong Top Dynamics

Models with new strong top dynamics fall into three general classes with distinctive spectra and phenomenology: topcolor,^{61,77} flavor-universal extended color,⁶² and top seesaw.⁷⁵ These theories include a variety of new states that can weigh less than a few TeV. A generic feature is colored gauge bosons with generation-specific (topgluon) or flavor-universal (coloron) couplings to quarks. The strongly-bound quarks may also form composite scalar states. Many models include color-singlet (Z') bosons with generation-dependent couplings. Some theories generate masses with the help of exotic fermions (usually, but not always weak-singlets). In this section of the talk, we review experimental searches for these new states.

Topcolor Models

The gauge structure of topcolor^{61,77} models, as outlined in section 2.5, generally includes extended color and hypercharge sectors (as in Eq. 33) and a standard weak gauge group. The third-generation fermions transform under the more strongly-coupled $SU(3)_h \times U(1)_h$ group, so that after the extended symmetry breaks to the SM gauge group the heavy topgluons and Z' couple preferentially to the third generation. The light fermions transform under $SU(3)_\ell \times U(1)_\ell$. CDF's search⁷⁸ for topgluons decaying to $b\bar{b}$ has put constraints on the topgluon mass for three different assumed widths (Figure 31); the topgluon's strong coupling to quarks ensures that it will be a rather broad resonance. Run II and the LHC should be sensitive to topgluons in $b\bar{b}$ or $t\bar{t}$ final states. The Z' , being more weakly coupled is narrow; CDF's

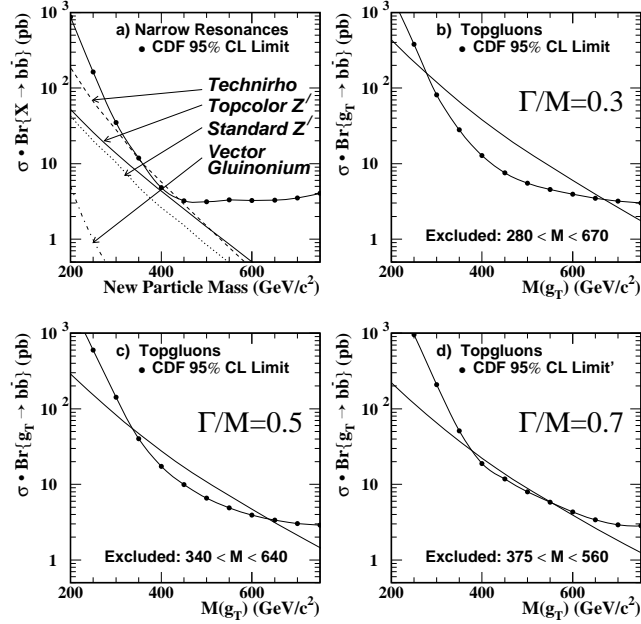


Figure 31. Results of CDF searches⁷⁸ for topgluons and Z' decaying to $b\bar{b}$.

limit on $\sigma \cdot B$ for narrow states⁷⁸ decaying to $b\bar{b}$ just misses being able to constrain this state (Figure 31). A more recent CDF search²⁹ for a leptophobic topcolor Z' decaying to top pairs excludes bosons weighing less than 480 (780) GeV assuming $\Gamma/M = 0.012$ (0.04). Precision electroweak data constrains⁷⁹ topcolor Z' bosons as shown in Figure 32; light masses are still allowed if the Z' couples almost exclusively to the third generation. As mentioned earlier, FNAL Run II will be sensitive⁶⁷ to topcolor Z' bosons as heavy as 750 GeV in the process $Z' \rightarrow \tau\tau \rightarrow e\mu X$. Ultimately, an NLC would be capable of finding a 3-6 TeV Z' decaying to taus.⁶²

The strong topcolor dynamics binds top and bottom quarks into a set of top-pions^{61,77} $t\bar{t}, t\bar{b}, b\bar{t}$ and $b\bar{b}$. It has been observed⁸⁰ that top-pion exchange in loops would noticeably decrease R_b (Figure 33) and this implies that the top-pions must be quite heavy unless other physics cancels this effect⁸¹. Several searches for top-pion and top-higgs (σ) states have been proposed. A singly-produced neutral top-higgs can be detected⁸² through its flavor-changing decays to tc at Run II. Charged top-pions, on the other hand,

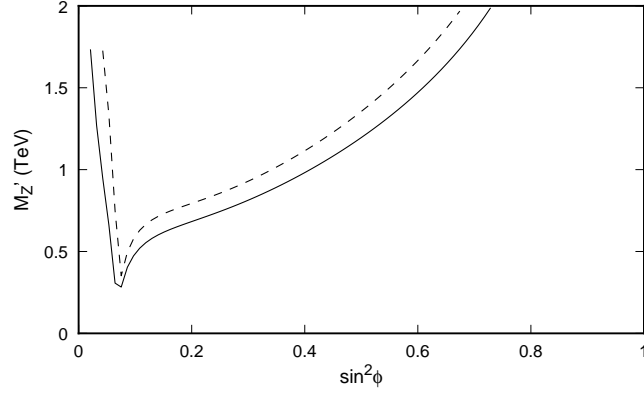


Figure 32. Lower bounds on the mass of topcolor Z' from precision electroweak data.⁷⁹

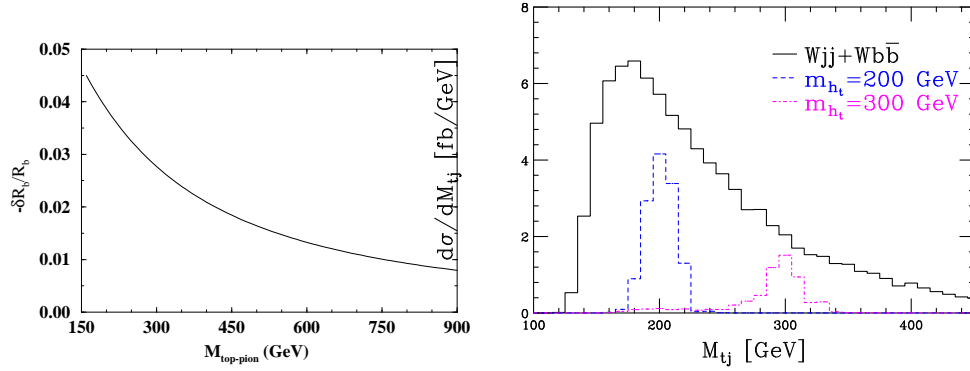


Figure 33. (left) Fractional reduction in R_b as a function of top-pion mass.⁸⁰ (right) Simulated signal and background for charged top-pions in the single top sample at the Tevatron.⁸³

would be visible⁸³ in single top production, as in Figure 33, up to masses of 350 GeV at Run II and 1 TeV at LHC.

Flavor-Universal Coloron Models

The gauge structure of these models⁶² is identical with that of the topcolor⁶¹ models; they differ only in fermion charge assignments. The

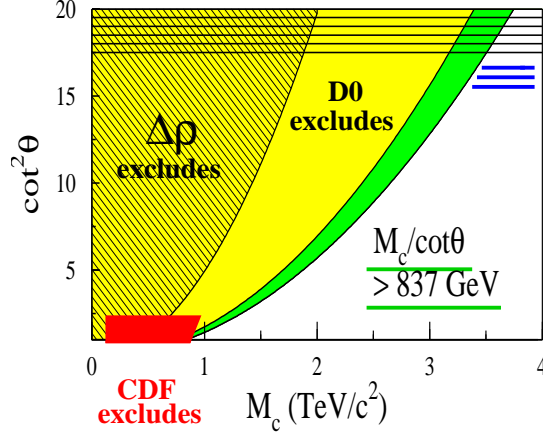


Figure 34. Limits⁸⁴ on the mass and mixing angle of flavor-universal colorons.

fermion hypercharges are as in topcolor models; hence, the Z' phenomenology is also the same. But as the model's name suggests, all quarks transform under the more strongly-coupled $SU(3)_h$ group; none transform under $SU(3)_\ell$. As a result, the heavy coloron bosons in the low-energy spectrum couple with equal strength to all quarks. Several experimental limits⁸⁴ have been placed on these color-octet states, as shown in Figure 34. CDF has excluded narrow colorons with masses below about 900 GeV by searching for resonances decaying to dijets. The bounds on $\Delta\rho$ exclude light colorons which could be exchanged across quark loops in weak boson propagators. Heavier colorons tend to be broad ($\Gamma \propto \kappa_3 M_c$) and therefore produce a distortion of the dijet angular distribution or excess events at high invariant mass, rather than a bump in the dijet spectrum. A $D\bar{O}$ study of the dijet angular distribution eliminated the light-shaded region of Figure 34 and a study⁸⁴ of the $D\bar{O}$ invariant mass distribution eliminated the darker-shaded slice, giving the limit $M_c/\cot\theta > 837$ GeV (where θ is the mixing angle between the two $SU(3)$ groups). This implies $M_c \gtrsim 3.4$ TeV in dynamical models of mass generation where the coloron coupling is strong.

In a TC2-like model incorporating flavor-universal colorons,⁶² the gauge couplings $\kappa_3 \equiv \alpha_s \cot^2 \theta_3$ and $\kappa_1 \equiv \alpha_Y \cot^2 \theta_1$ must satisfy several constraints which are summarized in Figure 35. Requiring solutions to the gauged NJL gap equations for dynamical fermion masses (Figure 36) such that only the

Table 4. Third generation quark charge assignments in top seesaw models.⁷⁵

	$SU(3)_h$	$SU(3)_\ell$	$SU(2)$
$(t, b)_L$	3	1	2
t_R, b_R	1	3	1
χ_L	1	3	1
χ_R	3	1	1

top quark condenses leads to the inequalities⁶²

$$\begin{aligned}
\kappa_3 + \frac{2}{27}\kappa_1 &\geq \frac{2\pi}{3} - \frac{4}{3}\alpha_s - \frac{4}{9}\alpha_Y & \langle t\bar{t} \rangle &\neq 0 \\
\kappa_3 + \frac{2}{27} \frac{\alpha_Y^2}{\kappa_1} &< \frac{2\pi}{3} - \frac{4}{3}\alpha_s - \frac{4}{9}\alpha_Y & \langle c\bar{c} \rangle &= 0 \\
\kappa_1 &< 2\pi - 6\alpha_Y & \langle \tau\tau \rangle &= 0
\end{aligned} \tag{35}$$

which form the outer triangle in Figure 35. Mixing between the Z and Z' alters the $Z\tau\tau$ coupling by^{79,62}

$$\delta g_{\tau_L} = \frac{1}{2}\delta g_{\tau_R} = \sin^2 \theta_W \frac{M_Z^2}{M_{Z'}^2} \left[1 - \frac{f_t^2}{v^2} \left(\frac{\kappa_1}{\alpha_Y} + 1 \right) \right] \tag{36}$$

where the top-pion decay constant is $f_t^2 = \frac{3}{8\pi^2} m_t^2 \ln \left(\frac{\Lambda^2}{m_t^2} \right)$. Keeping $Z \rightarrow \tau\tau$ consistent with experiment yields the upper bound labeled (5). Both ZZ' mixing and coloron exchange contribute^{79,62} to $\Delta\rho$

$$\begin{aligned}
\Delta\rho_*^{(C)} &\approx \frac{16\pi^2\alpha_Y}{3\sin^2\theta_W} \left(\frac{f_t^2}{M_C M_Z} \right)^2 \kappa_3 \\
\Delta\rho_*^{(Z')} &\approx \frac{\alpha_Y \sin^2\theta_W}{\kappa_1} \frac{M_Z^2}{M_{Z'}^2} \left[1 - \frac{f_t^2}{v^2} \left(\frac{\kappa_1}{\alpha_Y} + 1 \right) \right]^2
\end{aligned} \tag{37}$$

yielding upper bound (4). Finally, requiring that the Landau pole of the strongly-coupled $U(1)_h$ group lie sufficiently far above the symmetry-breaking scale M yields the curves labeled (6a,b,c) according to whether the separation of scales is by a factor of 10, 10^2 , or 10^5 . The combined limits⁶² indicate that the coloron coupling is not far below critical ($\kappa_3 \sim 1.9$) while $\kappa_1 \lesssim 1$. Similar constraints exist⁷⁷ for the original TC2 models.

Top Seesaw Models

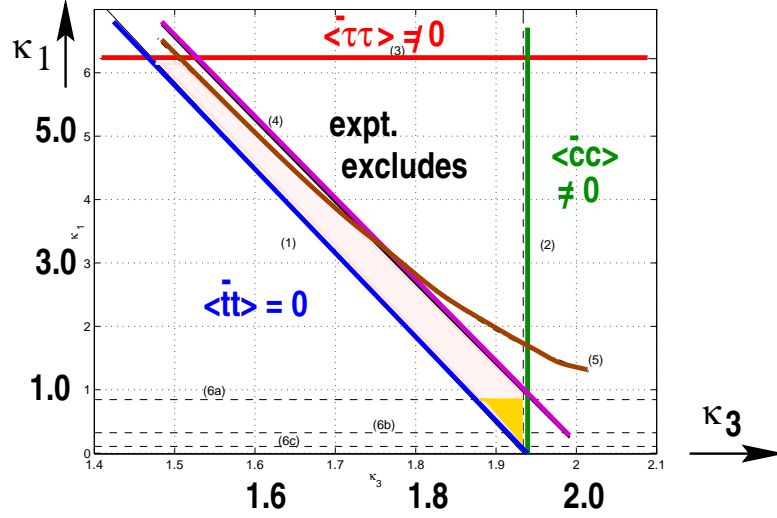


Figure 35. Limits on the coupling strengths κ_3 and κ_1 in flavor-universal coloron models.⁶²

$$\frac{\Sigma(p)}{x} = \frac{m_0}{x} + \text{loop with } x \text{ and } x \text{ lines} + \text{loop with } x \text{ and } x \text{ lines} + \dots$$

Figure 36. NJL gap equation for dynamical generation of fermion mass.

Top seesaw models⁷⁵ include an extended $SU(3)_h \times SU(3)_\ell$ color group which spontaneously breaks to $SU(3)_{QCD}$ while the electroweak gauge sector is standard. In addition to the ordinary quarks, there exist weak-singlet quarks χ which mix with the top quark; some variants^{85,65} include weak-singlet partners for the b, or for all quarks, or weak-doublet partners for some quarks. The color and weak quantum numbers of the third-generation quarks are shown in Table 4. When the $SU(3)_h$ coupling becomes strong, the dynamical mass of the top quark is created through a combination of $t_L \chi_R$ condensation and seesaw mixing:

$$\begin{array}{c} \bar{t}_L \quad \chi_R \quad \chi_L \quad t_R \\ \text{---} \quad \text{---} \quad \text{---} \quad \text{---} \end{array} \quad \left(\bar{t}_L \quad \bar{\chi}_L \right) \begin{pmatrix} 0 & m_{t\chi} \\ \mu_{\chi t} & \mu_{\chi\chi} \end{pmatrix} \begin{pmatrix} t_R \\ \chi_R \end{pmatrix} \quad (38)$$

Composite scalars $\bar{t}_L \chi_R$ are also created by the strong dynamics.

The phenomenology of the weak singlet quarks has received some atten-

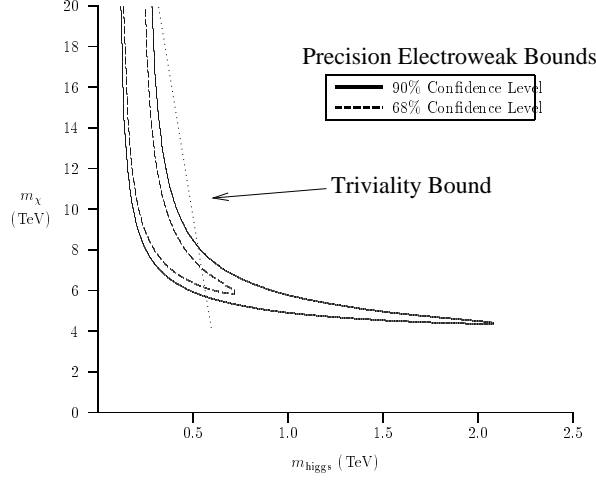


Figure 37. Electroweak⁸⁵ and triviality⁸⁶ bounds on the masses of the exotic quarks and composite scalars in a top seesaw model. The allowed region is within the banana-shaped region and to the left of the diagonal line.

tion in the literature. Experimental limits on weak isospin violation ($\Delta\rho$) provide a key constraint on models in which top has a weak-singlet partner and bottom does not. Even including a weak-singlet partner for the b quark cannot altogether alleviate this, as data on R_b limits the mixing between b and its partner. A combination of precision electroweak bounds and triviality considerations limits the χ quarks and the composite scalar to the mass range shown Figure 37. The exotic quarks are required⁸⁵ to have masses in excess of about 5 TeV. Note that the upper bound on the scalar mass from electroweak constraints at lower values of M_χ is looser than in the SM because⁸⁶ the model constrains extra contributions to $\Delta\rho$.

Direct searches for weak-singlet quarks are limited to lower mass ranges; while they cannot probe the partner of the top, they are potentially sensitive to weak-singlet partners of the lighter quarks. For example, a heavy mostly-weak-singlet quark q^H could contribute⁸⁷ to the FNAL top dilepton sample via

$$p\bar{p} \rightarrow q^H \bar{q}^H \rightarrow q^L W \bar{q}^L W \rightarrow q^L \bar{q}^L \ell \nu_\ell \ell' \nu_{\ell'} \quad (39)$$

Comparing the number of dilepton events to the SM prediction yields a lower bound on M_{q^H} . The limits will be weaker than that for a sequential 4th

generation quark because the mostly-singlet q^H do not always decay via the charged-current weak interactions. The d^H branching fraction to $d^H \rightarrow Wu^H$ is only about 60% due to competition from the flavor-conserving neutral current process $d^H \rightarrow Zd^L$. In the case of b^H , the cross-generation charged-current decay is also Cabibbo suppressed and the channel $b^H \rightarrow Zb^L$ dominates. As a result, Run 1 data places the limit⁸⁷ $M_{s^H, d^H} \gtrsim 140$ GeV, but cannot directly constrain M_{b^H} . In models where all three generations of quarks have weak-singlet partners, self-consistency requires⁸⁷ $M_{b^H} \gtrsim 160$ GeV.

2.7 Summary

The quest for understanding electroweak symmetry breaking and fermion masses points to physics beyond the SM. In many theories, the top quark is predicted to have unusual properties accessible to experiments at the Fermilab Tevatron's Run II, the LHC or an NLC. New physics associated with the top quark might include new gauge interactions or decay channels, exotic fermions mixing with top, a light supersymmetric partner, strongly-bound top-quark states, or something not yet even imagined. Studying the top quark clearly has tremendous potential to produce results that will be surprising and enlightening.

Acknowledgments

The author thanks R.S. Chivukula and S. Willenbrock for very useful comments on the manuscript. She also acknowledges the support of the NSF POWRE and RAIS Bunting Fellowship programs. *This work was supported in part by the National Science Foundation under grant PHY-0074274 and by the Department of Energy under grant DE-FG02-91ER40676.*

References

1. M.L. Perl *et al.*, *Phys. Rev. Lett.* **35**, 1489 (1975)
2. S.W. Herb *et al.*, *Phys. Rev. Lett.* **39**, 252 (1977)
3. E. Rice *et al.*, *Phys. Rev. Lett.* **48**, 906 (1982)
4. W. Bartel *et al.*, *Phys. Lett. B* **146**, 437 (1984)
5. C. Campagnari and M. Franklin, *Rev. Mod. Phys.* **69**, 137 (1997)
6. F. Abe *et al.*, *Phys. Rev. Lett.* **74**, 2662 (1995)
7. S. Abachi *et al.*, *Phys. Rev. Lett.* **74**, 2632 (1995)
8. S. Willenbrock, Studying the top quark, hep-ph/0008189.

9. F. Abe *et al.* *Phys. Rev. Lett.* **80**, 2767 (1998); *Phys. Rev. Lett.* **80**, 2779 (1998); *Phys. Rev. Lett.* **82**, 271 (1999)
10. S. Abachi *et al.* *Phys. Rev. Lett.* **79**, 1197 (1997); B. Abbott *et al.* *Phys. Rev. Lett.* **80**, 2063 (1998); *Phys. Rev. D* **58**, 052001 (1998); *Phys. Rev. D* **60**, 052001 (1999)
11. G. Watts, Talk given at Heavy Flavours 8, Southampton, England, July 25-29, 1999. <http://www-d0.fnal.gov/~gwatts/outside/hf8/>
12. D.E. Groom *et al.*, *E. Phys. J. C* **C15**, 1 (2000)
13. G. Degrassi, *et al.*, *Phys. Lett. B* **418**, 209 (1998)
14. LEP Electroweak Working Group, <http://lepewwg.web.cern.ch/LEPEWWG/>
15. P. Comas *et al.*, Recent Studies on Top Quark Physics at NLC, Proc. Iwate Linear Colliders, eds. A. Miyamoto, Y. Fujii, T. Matsui, and S. Iwata (World Scientific, 1996), p. 455.
16. M.C. Smith and S.S. Willenbrock, *Phys. Rev. Lett.* **79**, 3825 (1997)
17. G. 't Hooft, in The Whys of Subnuclear Physics, Proc. Int'l. School of Subnuclear Physics, Erice, 1997, ed. A. Zichichi (Plenum, NY, 1979), p. 943; Z. Mueller, in QCD - 20 Years Later, Proc. Workshop, Aachen, Germany, 1992, eds. P. Zerwas and H. Kastrup (World Scientific, Singapore, 1993), V. 1, p. 162.
18. M. Beneke and V. Braun, *Nucl. Phys. B* **426**, 301 (1994); I Bigi *et al.*, *Phys. Rev. D* **50**, 2234 (1994)
19. A.H. Hoang *et al.*, *E. Phys. J. C* **3**, 1 (2000)
20. M. Beneke, *Phys. Lett. B* **434**, 115 (1998)
21. I Bigi *et al.*, *Phys. Rev. D* **56**, 4017 (1997)
22. A.H. Hoang and T. Teubner, *Phys. Rev. D* **60**, 114027 (1999)
23. M. Beneke *et al.*, Top Quark Physics, hep-ph/0003033.
24. A.H. Hoang, Top Physics at the LC, presented at the Thinkshop 2 on Top Quark Physics for Run II & Beyond, Fermilab, Batavia, IL, November 10-12, 2000.
25. F. Abe *et al.*, *Phys. Rev. Lett.* **80**, 2773 (1998)
26. S. Abachi *et al.*, *Phys. Rev. Lett.* **79**, 1203 (1997)
27. E. Laenen, J. Smith, and W.L. van Neerven, *Phys. Lett. B* **321**, 254 (1994); E. Berger and H. Contopangonios, *Phys. Rev. D* **57**, 253 (1998); R. Bociani *et al.*, *Nucl. Phys. B*, 5 (2)94241998
28. B. Abbott *et al.*, *Phys. Rev. Lett.* **82**, 2457 (1999)
29. T. Affolder *et al.*, *Phys. Rev. Lett.* **85**, 2062 (2000)
30. T. Affolder *et al.*, Measurement of the Top Quark p(t) Distribution, Fermilab-Pub-00/101, 2000.
31. D. Amidei and R. Brock, eds., Future ElectroWeak Physics at the Fermilab Tevatron: Report of the TeV2000 Study Group, Fermilab-Pub-

- 96/046. <http://www-theory.fnal.gov/TeV2000.html> .
32. V. Barger, J. Ohnemus, and R. Phillips, *Int. J. Mod. Phys. A* **4**, 617 (1989)
 33. I. Bigi *et al.*, *Phys. Lett. B* **181**, 157 (1986)
 34. M. Jezabek and J.H. Kuhn, *Phys. Lett. B* **329**, 317 (1994)
 35. S. Parke and Y. Shadmi, *Phys. Lett. B* **387**, 199 (1996)
 36. T. Stelzer and S. Willenbrock, *Phys. Lett. B* **374**, 169 (1996)
 37. Y. Hara, *Prog. Theor. Phys.* **86**, 779 (1991)
 38. G. Mahlon and S. Parke, *Phys. Lett. B* **411**, 173 (1997)
 39. B. Abbott *et al.*, *Phys. Rev. Lett.* **85**, 256 (2000)
 40. M.C. Smith and S. Willenbrock, *Phys. Rev. D* **54**, 6696 (1997); T. Stelzer, Z. Sullivan, and S. Willenbrock, *Phys. Rev. D* **56**, 5919 (1997)
 41. B. Abbott *et al.*, Search for electroweak production of single top quarks in $p\bar{p}$ collisions, hep-ex/0008024 .
 42. L. Dudko, Search for Single Top Quark Production at the Tevatron, Proc. 35th Rencontres de Moriond, Les Arcs, France, March 11-18, 2000.
 43. T. Affolder *et al.*, *Phys. Rev. Lett.* **84**, 216 (2000)
 44. K. Tollefson, CDF Collaboration, Fermilab-Conf-98/389-E, 1998.
 45. F. Abe *et al.*, *Phys. Rev. Lett.* **80**, 2525 (1998)
 46. For a review of supersymmetry, consult: H. Murayama in these TASI-2000 lectures; or S. Dawson, SUSY and Such, hep-ph/9712464.
 47. G. Anderson, D. Castano, and A. Riotto, *Phys. Rev. D* **55**, 2950 (1997); H. Murayama and M. Peskin, *Ann. Rev. Nucl. Part. Sci.* **46**, 533 (1996)
 48. For a review of dynamical electroweak symmetry breaking, consult: R.S. Chivukula in these TASI-2000 lectures or in Models of Electroweak Symmetry Breaking, hep-ph/9803219; or K.Lane, Technicolor 2000, hep-ph/0007304.
 49. See, for example, the “experimental symptoms of new top physics” list located at <http://b0nd10.fnal.gov/regina/thinkshop/ts.html>
 50. For a review, see J. Gunion *et al.* The Higgs Hunter’s Guide, (Addison-Wesley, 1990).
 51. B. Abbott *et al.*, *Phys. Rev. Lett.* **82**, 4975 (1999)
 52. S. Snyder, Proc. EPS-HEP 99, Tampere, Finland, 15-21 July 1999, hep-ex/9910029.
 53. M. Machacek and M. Vaughn, *Nucl. Phys. B* **222**, 83 (1983); C. Ford *et al.*, *Nucl. Phys. B* **395**, 17 (1993)
 54. L. Ibanez, *Nucl. Phys. B* **218**, 514 (1983); L. Ibanez and G. Ross, *Phys. Lett. B* **110**, 215 (1982); J. Ellis, D. Nanopoulos, and K. Tamvakis, *Phys. Lett. B* **121**, 123 (1983); L. Alvarez-Gaume, J. Polchinski and M. Wise, *Nucl. Phys. B* **221**, 495 (1983); B. Ananthanarayan, G. Lazarides, and

- Q. Shafi, *Phys. Rev. D* **44**, 1613 (1991)
55. V. Barger, M. Berger and P. Ohmann, *Phys. Rev. D* **49**, 4908 (1994)
 56. P. Chankowski, S. Pokorski, and J. Rosiek, *Phys. Lett. B* **274**, 191 (1992); *Phys. Lett. B* **281**, 100 (1992); Y. Okada, M. Yamaguchi, and T. Yanagida, *Prog. Theor. Phys.* **85**, (1991); *Phys. Lett. B* **262**, 54 (1991); J. Espinosa and M. Quiros, *Phys. Lett. B* **267**, 27 (1991); *Phys. Lett. B* **266**, 389 (1991); H. Haber and R. Hempfling, *Phys. Rev. D* **48**, 4280 (1993); *Phys. Rev. Lett.* 6618151991; J. Gunion and A. Turski, *Phys. Rev. D* **39**, 2701 (1989); *Phys. Rev. D* **40**, 2333 (1990); M. Berger, *Phys. Rev. D* **41**, 225 (1990); K. Sasaki, M. Carena and C. Wagner, *Nucl. Phys. B* **381**, 66 (1992); R. Barbieri and M. Frigeni, *Phys. Lett. B* **258**, 395 (1991); J. Ellis, G. Ridolfi and F. Zwirner, *Phys. Lett. B* **257**, 83 (1991); 262 **477**, 1991 (; R. Hempfling and A. Hoang, *Phys. Lett. B* **331**, 99 (1994); R. Barbieri, F. Caravaglios, and M. Frigeni, *Phys. Lett. B* **258**, 167 (1991); H. Haber, R. Hempfling, and H. Hoang, *Z. Phys. C* **75**, 539 (1997); M. Carena, M. Quiros, and C. Wagner, *Nucl. Phys. B* **461**, 407 (1996); M. Carena *et al.*, *Phys. Lett. B* **355**, 209 (1995)
 57. T. Affolder *et al.*, *Phys. Rev. Lett.* **84**, 5704 (2000); *Phys. Rev. Lett.* **84**, 5273 (2000)
 58. R. Demina *et al.*, *Phys. Rev. D* **62**, 035011 (2000)
 59. G.L. Kane and S. Mrenna, *Phys. Rev. Lett.* **77**, 3502 (1996); G. Mahlon and G.L. Kane, *Phys. Rev. D* **55**, 2779 (1997); M. Hosch *et al.*, *Phys. Rev. D* **58**, 034002 (1998)
 60. R.S. Chivukula, E.H. Simmons, and J. Terning, *Phys. Lett. B* **331**, 383 (1994)
 61. C.T. Hill, *Phys. Lett. B* **266**, 419 (1991); S.P. Martin, *Phys. Rev. D* **45**, 4283 (1992); *Phys. Rev. D* **46**, 2197 (1992); *Nucl. Phys. B* **398**, 359 (1993); M. Lindner and D. Ross, *Nucl. Phys. B* **370**, 30 (1992); R. Bonisch, *Phys. Lett. B* **268**, 394 (1991); C.T. Hill *et al.*, *Phys. Rev. D* **47**, 2940 (1993); C.T. Hill, *Phys. Lett. B* **345**, 483 (1995); R.S. Chivukula and H. Georgi, *Phys. Rev. D* **58**, 115009 (1998); *Phys. Rev. D* **58**, 075004 (1998)
 62. R.S. Chivukula, A.G. Cohen, and E.H. Simmons, *Phys. Lett. B* **380**, 92 (1996); M.B. Popovic and E.H. Simmons, *Phys. Rev. D* **58**, 095007 (1998); K. Lane, *Phys. Lett. B* **433**, 96 (1998)
 63. R.S. Chivukula, S.B. Selipsky, and E.H. Simmons, *Phys. Rev. Lett.* **69**, 575 (1992); R.S. Chivukula *et al.*, *Phys. Lett. B* **311**, 157 (1993)
 64. D.J. Muller and S. Nandi, *Phys. Lett. B* **383**, 345 (1996); E. Malkawi, T. Tait, and C.-P. Yuan, *Phys. Lett. B* **385**, 304 (1996)
 65. G. Burdman and N. Evans, *Phys. Rev. D* **59**, 115005 (1999); H.-J. He,

- T. Tait, and C.P. Yuan, *Phys. Rev. D* **62**, 011702 (2000)
66. R.S. Chivukula, E.H. Simmons, and J. Terning, *Phys. Rev. D* **53**, 5258 (1996)
67. K.R. Lynch, *et al.*, *Phys. Rev. D* to appear. hep-ph/0007286
68. A.P. Heinson, Proc. 31st Rencontres de Moriond, Les Arcs, France, March 23-30, 1996; A.P. Heinson, A.S. Belyaev and E.E. Boos, *Phys. Rev. D* **56**, 3114 (1997); M.C. Smith and S. Willenbrock, *Phys. Rev. D* **54**, 6696 (1996)
69. E.H. Simmons, *Phys. Rev. D* **55**, 5494 (1997)
70. B.W. Lynn, Michael E. Peskin, R.G. Stuart, Radiative Corrections in $SU(2)$ Proc. of LEP Physics Workshop, CERN Report 1985; M.B. Einhorn, D.R.T. Jones, and M. Veltman, *Nucl. Phys. B* **191**, 146 (1981); M. Peskin and T. Takeuchi, *Phys. Rev. D* **46**, 381 (1992)
71. T. Appelquist *et al.*, *Phys. Rev. Lett.* **53**, 1523 (1984); *Phys. Rev. D* **31**, 1676 (1985)
72. R.S. Chivukula, *Phys. Rev. Lett.* **61**, 2657 (1988)
73. R.S. Chivukula, A.G. Cohen, and K.D. Lane, *Nucl. Phys. B* **343**, 554 (1990)
74. V.A. Miransky, M. Tanabashi and K. Yamawaki, *Phys. Lett. B* **221**, 177 (1989); *Mod. Phys. Lett. A* **4**, 1043 (1989); Y. Nambu, EFI-89-08 (1989) unpublished; W. Marciano, *Phys. Rev. Lett.* **62**, 2793 (1989); W.A. Bardeen, C.T. Hill, and M. Lindner, *Phys. Rev. D* **41**, 1647 (1990)
75. B.A. Dobrescu and C.T. Hill, *Phys. Rev. Lett.* **81**, 2634 (1998); R.S. Chivukula *et al.*, *Phys. Rev. D* **59**, 075003 (1999)
76. Y. Nambu and G. Jona-Lasinio, *Phys. Rev.* **122**, 345 (1961) ; *Phys. Rev.* **124**, 246 (1961)
77. R.S. Chivukula, B.A. Dobrescu, and J. Terning *Phys. Lett. B* **353**, 289 (1995); K. Lane and E. Eichten, *Phys. Lett. B* **352**, 382 (1995); K. Lane, *Phys. Rev. D* **54**, 2204 (1996); G. Buchalla *et al.*, *Phys. Rev. D* **53**, 5185 (1996); K. Lane, *Phys. Lett. B* **433**, 96 (1998)
78. F. Abe *et al.*, *Phys. Rev. Lett.* **82**, 2038 (1999).
79. R.S. Chivukula and J. Terning, *Phys. Lett. B* **385**, 209 (1996)
80. G. Burdman, *Phys. Lett. B* **403**, 101 (1997)
81. C.-X. Yue *et al.* *Phys. Rev. D* **62**, 055005 (2000)
82. G. Burdman, *Phys. Rev. Lett.* **83**, 2888 (1999)
83. H.-J. He and C.P. Yuan, *Phys. Rev. Lett.* **83**, 28 (1999)
84. I.A. Bertram and E.H. Simmons, *Phys. Lett. B* **443**, 347 (1998); E.H. Simmons, *Phys. Rev. D* **55**, 1678 (1997)
85. H. Collins, A. Grant, and H. Georgi, *Phys. Rev. D* **61**, 055002 (2000)
86. R.S. Chivukula and N. Evans, *Phys. Lett. B* **464**, 244 (1999); R.S.

- Chivukula, N. Evans, and C. Hoelbling, *Phys. Rev. Lett.* **85**, 511 (2000)
87. M. Popovic and E.H. Simmons, *Phys. Rev. D* **62**, 035002 (2000)